Trends in Analytical Chemistry 181 (2024) 117991

Contents lists available at ScienceDirect

Trends in Analytical Chemistry

journal homepage: www.elsevier.com/locate/trac

Laser-induced breakdown spectroscopy in space applications: Review and prospects

H. Saeidfirozeh [a], P. Kubelík [a], V. Laitl [a,b], A. Křivková [a,c], J. Vrábel [d,e], K. Rammelkamp [f], S. Schröder [f], I.B. Gornushkin [g], E. Képeš [e], J. Žabka [a], M. Ferus [a,**], P. Pořízka [d,e,h,*], J. Kaiser [d,e,h]

[a] J. Heyrovský Institute of Physical Chemistry, Czech Academy of Sciences, Dolejškova 3, CZ 18223, Prague 8, Czech Republic
[b] University of Antwerp, Faculty of Science, Groenenborgerlaan 171, BE-2020 Antwerpen, Belgium
[c] Czech Technical University in Prague, Faculty of Nuclear Sciences and Physical Engineering, Břehová 78/7, 11519, Prague 1, Czech Republic
[d] Central European Institute of Technology, Brno University of Technology, Purkyňova 656/123, CZ-61200, Brno, Czech Republic
[e] Institute of Physical Engineering, Faculty of Mechanical Engineering, Brno University of Technology, Technická 2, CZ-61669, Brno, Czech Republic
[f] Institute of Optical Sensor Systems, German Aerospace Center (DLR), DE-12489, Berlin, Germany
[g] BAM Federal Institute for Materials Research and Testing Richard-Willstaetter-Strasse 11, 12489, Berlin, Germany
[h] Lightigo Space s.r.o., Renneská třída 329/13, CZ-63900, Brno, Czech Republic

ARTICLE INFO

Keywords:
Laser-induced breakdown spectroscopy
Mars
Moon
Asteroids
Meteorites
Machine learning
Transfer learning
Raman spectroscopy
Mass spectrometry
Fourier-transform infrared spectroscopy

ABSTRACT

This review describes the principles and summarizes the challenges of analytical methods based on optical emission spectroscopy (OES) in space applications, with a particular focus on Laser-Induced Breakdown Spectroscopy (LIBS). Over the past decade, LIBS has emerged as a powerful analytical technique for space exploration and In-Situ Resource Utilization (ISRU) of celestial bodies. Its implementation has been suggested for various segments of the Space Resources Value Chain, including prospecting, mining, and beneficiation. Current missions to Mars, including the ChemCam instrument on the Curiosity rover, the SuperCam on the Perseverance rover, and the MarSCoDe on the Zhurong rover, are considered flagship applications of LIBS. Despite neither the Pragyan rover nor the Vikram lander waking from the lunar night, the success of the Chandrayaan-3 mission marks another milestone in the development of LIBS instruments, with further missions, including commercial ones, anticipated.

This paper reviews the deployment of LIBS payloads on Mars rovers, upcoming missions prospecting the Moon and asteroids, and LIBS analysis of meteorites. Additionally, it highlights the importance of data processing specific to space applications, emphasizing recent trends in transfer learning. Furthermore, LIBS combined with other spectroscopic techniques (e.g., Raman Spectroscopy, Mass Spectrometry, and Fourier-Transform Infrared Spectroscopy) represents an intriguing platform with comprehensive analytical capabilities. The review concludes by emphasizing the significance of LIBS-based contributions in advancing our understanding of celestial bodies and paving the way for future space exploration endeavors.

1. Introduction

Recent years have witnessed the emergence of Laser-Induced Breakdown Spectroscopy (LIBS) as a powerful tool for space research, offering a non-invasive, remote, rapid, and versatile method for elemental analysis in missions to the Moon, Mars, and potentially in future explorations beyond these celestial bodies [1–3]. Shortly after the successful construction of the first laser by Maiman in 1960, laser-induced plasma was observed, and the first analytical application for the spectrochemical analysis of surfaces was published; see Ref. [4] and the references therein for more details.

The application of lasers for remote analysis was first suggested in the 1980s [5]. By 1989, a 1-J laser system was integrated onboard the Soviet Phobos 2 mission to ablate material from the Martian moon Phobos from a distance of 80 m. The ablated material was then supposed to be analyzed by a time-of-flight mass spectrometer on the spacecraft.

* Corresponding author. Central European Institute of Technology, Brno University of Technology, Purkyňova 656/123, CZ-61200, Brno, Czech Republic.
** Corresponding author.
E-mail addresses: martin.ferus@jh-inst.cas.cz (M. Ferus), Pavel.Porizka@ceitec.vutbr.cz (P. Pořízka).

https://doi.org/10.1016/j.trac.2024.117991
Received 26 April 2024; Received in revised form 9 August 2024; Accepted 30 September 2024
Available online 9 October 2024
0165-9936/© 2024 Published by Elsevier B.V.

However, contact with the probe was lost during the approach manoeuvre. In 1992, Cremers et al. published pioneering works supporting the fees, such ability of LIBS in lunar missions, highlighting its potential for real-time remote analysis onboard a rover for distant objects [6]. This line of research culminated in a systematic study published in 2000 [7], followed by the first real mission application of LIBS system onboard the Curiosity rover in 2012 [2,8,9].

Mars missions [1,10–13] highlighted all the LIBS advantages: The technique is minimally destructive, rapid, and enables remote analysis without the need for sample preparation (such as brushing, polishing, or cleaning). It holds the promise of assisting in the selection of landing sites, identification of resources, and examination of celestial body geology. These attributes establish it as a crucial tool for real-time elemental analysis onboard other space missions of rovers and landers to the Moon, Venus, asteroids, and beyond.Recently, LIBS has also demonstrated its value in laboratory investigations of extraterrestrial materials, as well as in the domains of laboratory astrophysics and astrochemistry. Specifically, it has been employed in studies investigating meteorites [15,16] and in analyzing samples returned from space missions [17], providing insights into the composition and origins of extraterrestrial materials. Additionally, LIBS has been employed as an auxiliary experimental technique in meteor spectroscopy, which is crucial for the remote elemental analysis of meteor plasma. This application is particularly important for studying interplanetary matter as it enters Earth's atmosphere at velocities high enough to cause heating and ablation of its surface [18].

This review examines the latest trends in applying Laser-Induced Breakdown Spectroscopy for space research. Initially, Section 2 provides an overview of LIBS techniques, assessing their viability and the challenges they face in space missions. Section 3 focuses on the application of LIBS on Mars, highlighting recent advancements and relevant considerations. Furthermore, Section 4 discusses the challenges and achievements in employing LIBS to analyze lunar regolith. In Section 5, our investigation extends to asteroids, examining LIBS's potential in the prospecting and analysis of meteorites. Throughout this exploration, emphasis is placed on data processing methodologies for LIBS, as discussed in Section 6. Additionally, an in-depth examination of modeling laser-induced plasmas under the atmospheric conditions of celestial bodies is presented in Section 7. Finally, Section 8 summarizes the advancements and applications of hyphenated LIBS methods.

2. Overview of laser-induced breakdown spectroscopy

In this section, we only marginally introduce the LIBS technique and its basic instrumental and experimental aspects. This is done for the sake of completeness and to put LIBS in a broader perspective for the audience beyond the LIBS community.

LIBS is a technique based on optical emission spectroscopy (OES), whose benefits make it a prominent candidate for In-Situ Resource Utilization (ISRU) of celestial bodies. The simplicity of LIBS is in its straightforward nature of laser ablation and OES probing of consequent Laser-Induced Plasma (LIP). Due to its instrumental robustness, LIBS has received significant attention in modern extraterrestrial exploration. The demand for accurate elemental analysis of various samples is provided through the measurement of electromagnetic radiation emitted by the relaxation of excited atoms or ions. These transitions mainly occur in the ultraviolet, visible, and infrared regions of the electromagnetic spectrum, thus typically covering the range of 130–850 nm [19]. Laser-induced plasma OES provides valuable information about the plasma parameters such as plasma temperature and electron number density, as well as about the specimens being probed; the latter's precision not only spans elemental analysis but, in certain cases, also isotope speciation [20].

As shown in Fig. 1, a typical LIBS setup requires three main parts: (i) a laser source, (ii) an optical system (incl. collection optics, spectrometer with detector), and (iii) a data processing unit.

The principle of the LIBS technique lies in focusing a laser pulse on the sample of interest, ablating a small amount of its material, and generating a laser-induced plasma from the vaporized mass above the sample surface. The selection of the laser type depends on the specific application and the elements of interest within the sample. Typical laser sources used in LIBS setup are pulsed Nd:YAG lasers [21,22]. The optical system typically constitutes two separate branches: (i) laser focusing and (ii) collection of LIP radiation.

For the sake of instrumental simplicity and robustness of the LIBS instruments, the optical system is a compact set of basic optical components (*e. g.*, focusing lens(es), mirrors, and a collimator). The focusing branch ensures that the focused laser pulse exceeds the above-threshold irradiance, whereas the collection branch is responsible for delivering the analytical signal with maximal optical throughput into the spectrometer. By processing the resultant emission spectra, LIBS enables rapid detection of a wide range of elements, including volatiles and light elements, which makes it particularly suitable for in-situ analysis in space missions.LIBS performance and analytical feedback are affected

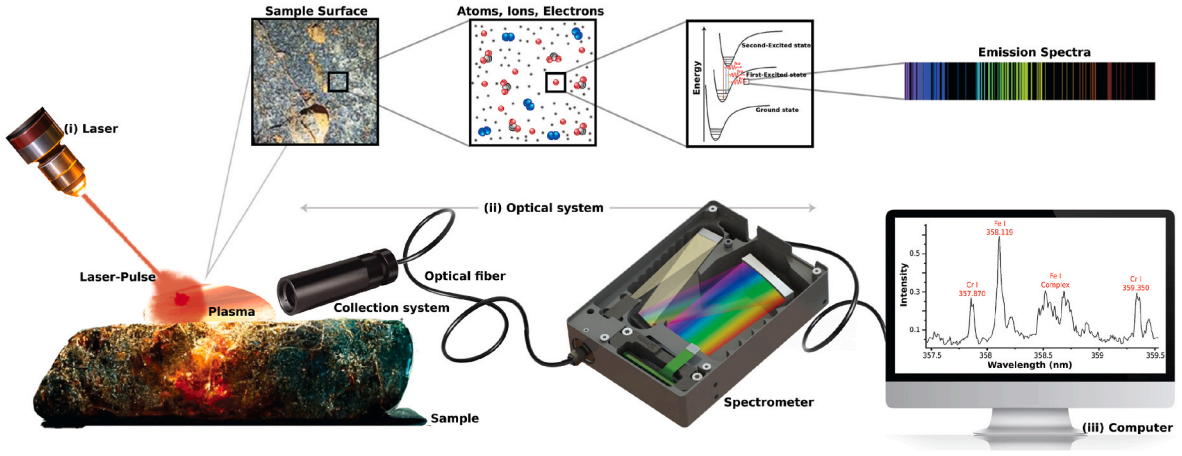

Fig. 1. The physical principle of Laser-Induced Breakdown Spectroscopy. It shows its main three parts: **(i)** a laser source, **(ii)** an optical system, and **(iii)** a data processing unit. The laser pulse is focused on the sample surface to ablate a small mass (ng $\sim \mu$g) and create a plasma, with a lifetime range from 300 ns to 40 µs [14], and temperatures often exceeding 10,000 K. During the cooling process of the plasma, excited atoms transit to a lower energy state by characteristic (discrete) emission. The emitted light by plasma is collected by the collection optics and passed to the spectrometer. The optical systems of space probing interest are detailed below, and the final data processing is delved into by Sec.6.

both by the experimental conditions and the sample's matrix effects. Especially from the perspective and scope of this review, the ambient conditions are of paramount interest. One major challenge, however, is the different atmospheric conditions encountered in space compared to terrestrial environments. For instance, as mentioned by Hahn et al. in their experimental studies [23], conducting LIBS measurements in conditions similar to the future possible Venus mission requires handling pressures as high as 90 atm and temperatures over 700 K [24]. Such conditions, although generally feasible for operating LIBS plasma in a (very) contracted mode, may be detrimental to the supporting apparatus. Besides, the high densities of Venus's atmosphere introduce noticeable interferences to geochemical measurements [25]. On the other hand, spaceborne LIBS is (to be) employed also in environments exhibiting reduced air pressures, as on Mars [26], or entirely lacking atmosphere, as on the Moon [27,28]. Such variations in ambient pressure and atmosphere composition significantly affect the LIBS results obtained [1,29]. On the one hand, upon pressure decrease, the spark plasma ceases contracting, which enhances nonequilibrium effects and complicates signal readout. On the other hand, with increasing pressure, the likelihood of background atmospheric interference grows. Case-specific adapting of instrumental setups and calibration procedures becomes thus essential [11,12,30]. We have compiled an overview in Table 1 to summarize the various environmental challenges, relevant instruments, and signal enhancement techniques employed in space exploration. This table provides a concise reference for understanding how different celestial environments impact LIBS operations and the adaptations required to ensure accurate analytical results.

From the analytical standpoint, in theory, such obstacles can be disburdened by a one-way abundance-to-signal calibration for the analytes of interest. However, space exploration presents limited hands-on calibration possibilities. Ideally, standards related to a given celestial body should be borne aboard the craft, which, however, is often not fully feasible due to size and cargo weight limits [31].

Limited room within the spacecraft dictates that only a few selected calibration targets can be accommodated, underscoring their critical importance in ensuring precise scientific measurements during interplanetary missions. For example, Fig. 2 shows calibration targets mounted aboard the Curiosity rover, representing their usage in space missions to monitor the quality of acquired LIBS spectra. Fig. 2(c) shows that this onboard target comprises nine circles of materials, including four glass samples representing Mars igneous rock compositions in the top row, along with a graphite rod. The bottom row features four ceramic samples representing Mars's sedimentary rock compositions and a titanium square for wavelength calibration and laser diagnostic tests [12].

Instrumental limitations are also crucial factors to consider [32] since miniaturizing the LIBS device may result in side effects pertaining to resolution, collection efficiency, or geometric constraints. Detailed understanding and accounting for all such effects are therefore imperative for accurately interpreting and quantifying the measured spectra. Moreover, the simulation of atmospheric conditions of selected celestial bodies demands advanced instrumentation, such as interaction chambers [33].

However, until now, there has been no commercially available solution that could meet the demands of space-related LIBS analyses.

In this review, we focus in detail on how such issues are dealt with in a well-explored Mars case. As a natural follow-up, various feasibility studies foresee LIBS greatly contributing to future Venus exploring missions [24,34,35]. Indeed, the difference in surface temperature and high atmospheric pressure on Venus present palpable challenges for any lander-based missions. In this context, LIBS instrumentation emerges as a valuable geo-analytical tool for future missions to the planet. Furthermore, the majority of LIBS methods come with the advantage of avoiding traditional sampling techniques, making laser-based analyses a natural choice for exploring the challenging Venus's environment. We thus foresee Venus's mission drawing upon recent Martian explorations to a large degree. Instead of further delving into planetary LIBS, therefore, further case applications are reviewed for such low-pressure objects as the Moon or asteroids. Finally, recent insights on space-relevant LIBS data processing, modelling, and analytical hyphenation are summarized.

Table 1
Overview of selected celestial bodies relevant to the scope of this paper, their environments, and related technical challenges. The table lists existing missions during which the LIBS payloads were successfully deployed. Note that specifics of LIBS under listed atmospheric conditions are reflected in the respective chapters of this paper.

Celestial Body	Environment challenges	Relevant Instruments
Moon	- deep vacuum conditions (down to 10^{-12} Torr) - extreme temperature variations (<170 °C to >120 °C) - radiation hardening (≈ 200 × higher dose than on Earth) - dust mitigation	- LIBS instrument (Pragyan rover, ISRO)
Mars	- CO_2-dominant atmosphere (≈ 5 Torr) - temperature variations (<70 °C to >20 °C) - dust storms and dust mitigation - radiation hardening (≈ 24 × higher dose than on Earth)	- ChemCam (Curiosity rover, NASA) - SuperCam (Perseverance rover, NASA) - MarsCoDe (Zhurong rover, CNSA)
Venus	- CO_2-dominant atmosphere with sulfuric acid clouds - high pressure (≈ 69,000 Torr) - consistent surface temperature (≈ 465 °C)	- potential future instruments
Asteroids (e.g., Ceres, Vesta)	- varied surface compositions - maneuvering challenges in low gravity - deep space vacuum conditions (down to 10^{-17} Torr) - surface temperature ranges <-30 °C	- potential future instruments

3. LIBS on mars: Recent results and future prospects

LIBS on Mars is a great success story, all instruments Fig. 3 (ChemCam, SuperCam, and MarsCoDe, all listed below) greatly contributed and are still contributing to the overall mission objectives. The Martian LIBS instruments also motivated many laboratory studies to support the interpretation of Martian LIBS data, to develop optimized data analysis methods, and to demonstrate the feasibility of such instruments. There are already new proposals for future LIBS instruments on Mars missions such as a light-weight payload capable of doing LIBS raster scans in close range of 20–50 cm [36].

3.1. ChemCam on the curiosity rover

The ambient conditions on the Martian surface with a pressure of about 700 Pa are close to ideal for LIBS measurements as they provide a good compromise between confinement of the LIBS plasma and a low density inside the plasma plume [37]. The first ensures a plasma lifetime of several μs and reduced plasma shielding, i.e. the laser pulse being partially absorbed by the evolving plasma, and enables LIBS data with high signal-to-noise ratios, while the latter reduces the effect of pressure broadening of the emission lines. And so it was that the first extraterrestrial LIBS instrument called ChemCam (*Chemistry and Camera*) was put to use in-situ on Mars [10,12]. ChemCam is part of the payload of NASA's Mars Science Laboratory (MSL) rover called *Curiosity* and has been exploring Gale crater since landing in August 2012 [38]. After 3, 700 sols (i.e. Martian days since landing) more than 930,000 single shot LIBS spectra from more than 3,500 unique rock and regolith targets were

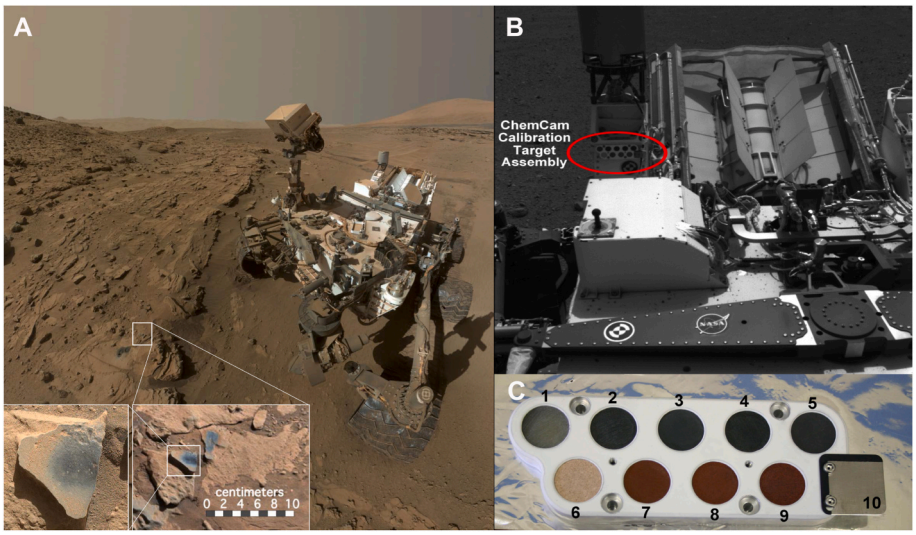

Fig. 2. **(A)** Selfie taken by the *Curiosity* rover at a location where the target *Stephen* was measured with ChemCam, shown in the zoom in the inset. Here the benefit of LIBS for space exploration can be clearly seen: a target at a remote distance is measured via optical access only with a precise pointing on a mm scale. **(B)** LIBS calibration on the on NASA's Curiosity rover. **(C)** Calibration target for the ChemCam. Photos courtesy of NASA.

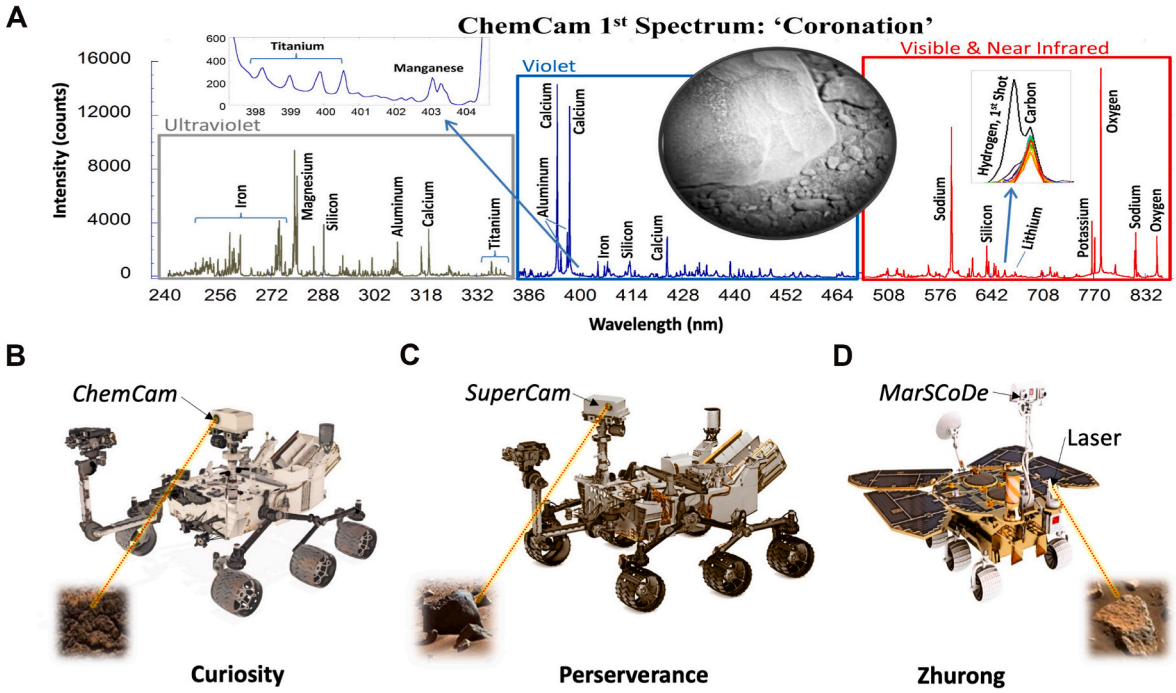

Fig. 3. **(A)** First extraterrestrial LIBS spectrum measured with ChemCam on the surface of Mars. The target is named *Coronation*, and its spectrum shows all emission lines of major rock-forming minerals as well as the decrease of the H emission line after a few shots corresponding to the dust removal by the shockwave of the LIBS plasma (Photo courtesy of NASA). Schematic of the **(B)** Curiosity, **(C)** Perseverance, **(D)** Zhurong rover.

acquired [39]. At the time of this writing, the rover has passed the 4,000 sols mark and continues to collect LIBS data from the surface of Mars. The ChemCam instrument comprises two sub-units: the mast unit (MU) [10] and the body unit (BU) [12] whose schematics are shown in Fig. 4 (A). The MU features a telescopic architecture with a 110-mm diameter aperture Schmidt-Cassegrain design that enables laser focusing and plasma emission collection, allowing for analysis of targets up to 7 m away from the instrument. The laser's active medium is an Nd:KGW crystal, emitting pulses at 1067 nm with pulse energies > 24 mJ at a frequency of 3 Hz. The laser was developed by Thales Optronic SA specifically for stand-off LIBS on the surface of Mars with constraints coming from the robotic platform and the expected environmental Martian conditions. The plasma emission is collected and guided through optical fibres into the BU. From there, it is directed with a demultiplexer into three Czerny-Turner spectrometers that cover the following spectral ranges: 240–342 nm (UV), 382–469 nm (VIO), and 474–907 nm (VNIR). CCDs are used as detectors, and read-out time per spectrum is about 13 ms, which is considerably longer than the plasma lifetime in Martian atmospheric conditions. Additionally to the LIBS system, ChemCam comprises the Remote Micro-Imager (RMI), which supports the geochemical data and their interpretation with high-resolution context images that are taken before and after the LIBS measurements [42]. There are, moreover, 10 dedicated LIBS calibration targets attached to the rover [43], which are measured by ChemCam for

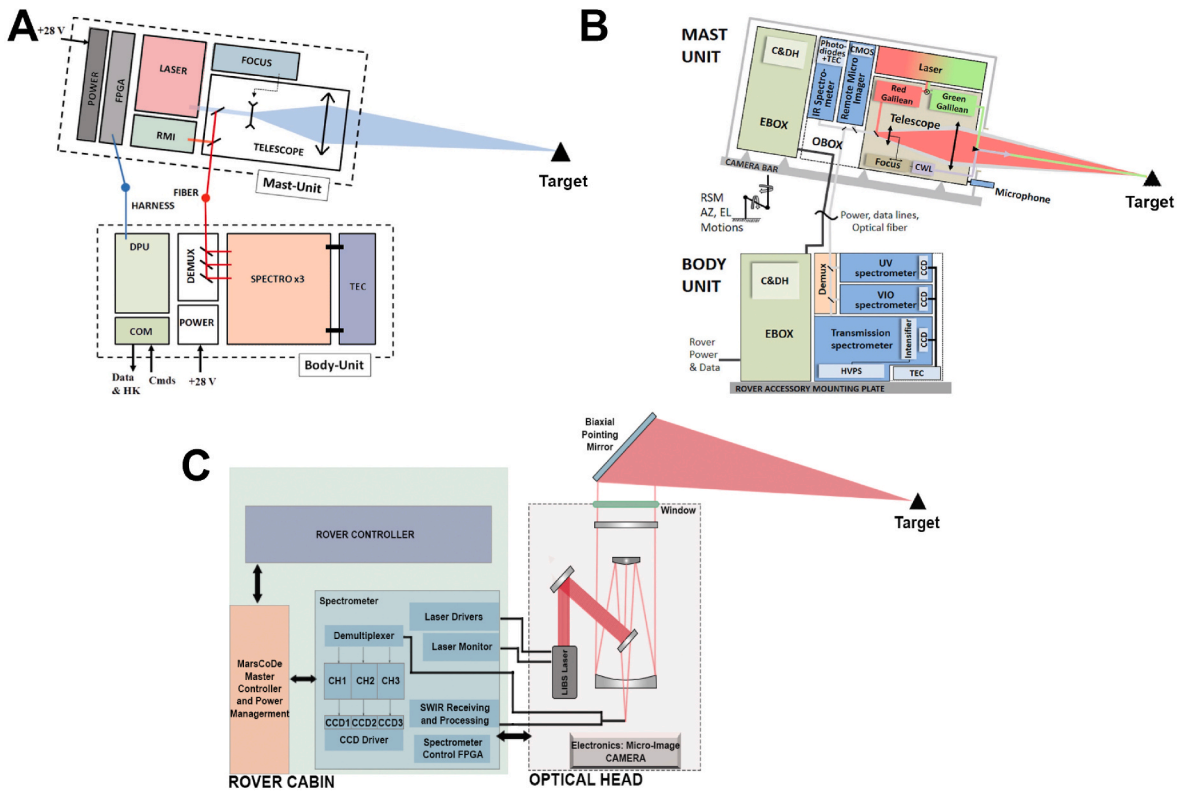

Fig. 4. Summary of Block diagram of (A) ChemCam [10], (B) SuperCam [40], (C) MarsCoDe (adapted from Ref. [41]) displaying the individual body and mast components along with their corresponding subsystems.

different aspects of calibration (Earth-to-Mars correction, wavelength calibration, quantification) and to track system performance.

ChemCam is a complex instrument with a total weight of 10 kg including a thermoelectric cooler (TEC) for the CCDs in the otherwise too-warm body of the rover. Before ChemCam operations, the TEC is used to cool the CCDs while parts in the MU, including the laser, need to be heated. An autofocus process adjusts the system with respect to the distance of the target of interest. An RMI image is then taken before the LIBS measurement. A measurement of a target typically consists of a raster of multiple analysis points (5–25) where at least 30 laser shots are taken at each position, resulting in 30 individual spectra along the depth of the LIBS crater. The spacing is typically in the order of 0.5 and 2 mrad, corresponding to several mm on the target. The laser spot size is in the range of 350–550 μm, depending on the distance of the target [13]. After the last LIBS measurement of the raster, a final RMI is taken, during which small ablation craters or dust movements can often be seen. For bigger rasters or rough surfaces, additional autofocusing and/or RMI images might be needed and be added to the sequence. After the measurement sequence, the TEC is turned off, the laser cooled and the mast pointed in a way that is sun-safe, protecting the instrument that features no cover from being damaged from sunlight. Measuring one LIBS raster is considered fast regarding the versatility and the space exploration-related measures as it requires around 30 min. Due to the long time needed for communications between Earth and Mars (several minutes), rover operation commands are prepared for entire sols or several sols in a row.

ChemCam has contributed significantly to the scientific discoveries of the MSL mission. On the one hand, the amount of data contributes to the characterization of the chemostratigraphy along the traverse of the rover, which completes the big picture and gives detailed compositions of all geological members visited so far [13,44–50]. Although the strata in Gale crater consists mainly of fine-grained sedimentary rocks, some igneous rocks, in particular at the beginning of the mission, could be analyzed, contributing to the identification of five igneous end-members [51,52]. ChemCam LIBS data was also used to characterize the soil and dust composition in Gale crater [53–55]. On the other hand, ChemCam's small laser spot size of 300–600 μm allows it to specifically analyze relatively small features. For example, diagenetic features such as veins, concretions, nodules, and halos [56–60] can be characterized, as well as small inclusions consisting of almost pure iron oxide on the Vera Rubin ridge [61,62]. Because of LIBS' sensitivity also to light elements, ChemCam detected for the first time the elements F [63] and B [64] in-situ on the surface of Mars. These elements can not be observed with techniques used on previous robotic platforms on Mars and their detection with ChemCam shows that the Martian surface composition is more diverse than assumed before. Interestingly, the first indication of the presence of F was the molecular emission band of CaF. Simple molecules can form temporarily in the LIBS plasma and sometimes have stronger bands in the spectra than the elementary emission lines, e.g. of the halogens F and Cl [65,66]. Furthermore, even though quantifying H abundances with LIBS is challenging due to the complex behavior of the lightest element, ChemCam was able to provide essential insight into the presence of hydrated minerals based on the LIBS H signal [67–69].

3.2. *SuperCam on the perseverance rover*

Due to the success of ChemCam, a follow-up instrument for NASA's Perseverance rover in the framework of the Mars2020 mission was suggested and selected: SuperCam [40,70]. Perseverance arrived at Jezero crater in February 2021 to explore, in particular, the deltaic formation seen in orbital data. Besides LIBS, SuperCam can do Raman-, fluorescence, and reflection spectroscopy, record sound, and take high-resolution RGB images. Although the interior design of the instrument differs in comparison to ChemCam, there are similarities in the architecture with two subsystems, MU and BU, schematically shown in Fig. 4(B). Besides the added capabilities, another enhancement in comparison to ChemCam, is that SuperCam carries an extended set of calibration targets [71] and operates a Nd:YAG laser with the typical

wavelength of 1064 nm. For Raman spectroscopy, this laser is frequency doubled to emit at 532 nm. As ChemCam, SuperCam has three spectrometers, but the VNIR one was replaced with a transmission spectrometer with a gated intensifier allowing time-resolved detection for the pulsed Raman measurements. The SuperCam microphone can be synchronized with the LIBS measurements and provides complementary data about coupling efficiencies and rock hardness [72]. With now more than 1000 sols on Mars, SuperCam measured many targets with all its techniques and significantly contributed to the scientific findings of the Mars2020 mission so far, e.g. Refs. [73–76].

3.3. MarsCoDe on Zhurong rover

In addition to the NASA missions, the CNSA's Tianwen-1 mission brought another LIBS instrument to Mars onboard the *Zhurong* rover called *MarsCoDe* [41]. Zhurong arrived on the Martian surface at Utopia Planitia in the northern lowlands in May 2021 and collected data until late 2022. Similar to the two LIBS instruments on the NASA rovers, MarsCoDe consists of two units, one on the inside of the rover and the other one outside of it (see Fig. 4(C)). The latter is an optical head with a Ritchey-Chretien telescope as a key component. In addition, for LIBS it used a laser which is passively Q-switched with a wavelength of 1064 nm, a repetition rate of 1–3 Hz emitting laser pulses of 4.5 ns duration and with 21 mJ. A biaxial pointing mirror sits on top of the optical head and enabled the instrument to measure targets at distances of 2–5 m. Besides LIBS measurements, *MarsCoDe* also took RMI images for context and collected the short-wave infrared (SWIR) part of the reflected light of the target. The other sub-unit in the inside of the rover contains a controller and the spectrometers. Via an optical fibre, the plasma radiation was guided to a demultiplexer which further splits it into three branches covering the spectral ranges 240–340 nm, 340–540 nm, and 540–850 nm. The instrument also carries a set of on-board calibration targets [77] and allowed, for example, to monitor spectral drifts due to instrumental temperature changes [78]. *MarsCoDe* data supported the characterization of the surface composition of rocks and soils at the *Zhurong* landing site in southern Utopia Planitia [79,80].

4. LIBS on the moon: Overcoming challenges for lunar regolith analysis

The attention of space exploration focuses back to the Moon with numerous robotic and crewed missions planned. Especially NASA's Artemis program will lead to a series of missions to reestablish the human presence on the Moon. Thus, the permanent presence of mankind on the Moon is not anymore just a vision but has become a strategy of many space agencies. This also attracts the private sector, while in the future, the prospecting and in-situ resources utilization (ISRU) [81] will open a completely new market, the so-called New Space.

The Moon is the most explored celestial body with diverse regions (highland, mare, and polar) of interest for ISRU [81–83]. The main source of interest is the prevalence of frozen water in the permanently frozen regions, lunar craters, in polar regions. However, the water content ranges widely (up to 15 %) as estimated by LCROSS and Chandrayaan-1 remote probes [84,85] and summarized in the mission concept of the LUVMI-X mission [86]. The exact characteristics of the form of water ice and its purity are also hard to estimate only from remote sensing, and a rover mission is mandatory for further prospecting. Moreover, other relevant elements of interest, incl. volatiles, are detectable through the utilization of LIBS which makes it a prominent technique for Moon exploration. Polar regions of the Moon have been the main areas of interest for ISRU, attracting various prospecting and extracting missions.

The prospecting of the Moon regolith interests many (inter)national and even commercial missions, Fig. 5. For all the missions, the instrumentation must be robust enough to withstand harsh lunar conditions, including temperature fluctuations, radiation, and high vacuum. Developing LIBS payloads that remain effective in such conditions is critical for its successful use in lunar exploration. Efforts towards in-situ deployment on the Moon were advanced with the Chandrayaan-2 mission, where a miniaturized, low-power LIBS instrument (weight ~1.1 kg, power consumption <1.2 W) was developed [87,88]. In August 2023, the Chandrayaan-3 rover, carrying a LIBS instrument, successfully landed near the lunar south pole, achieving the first in-situ

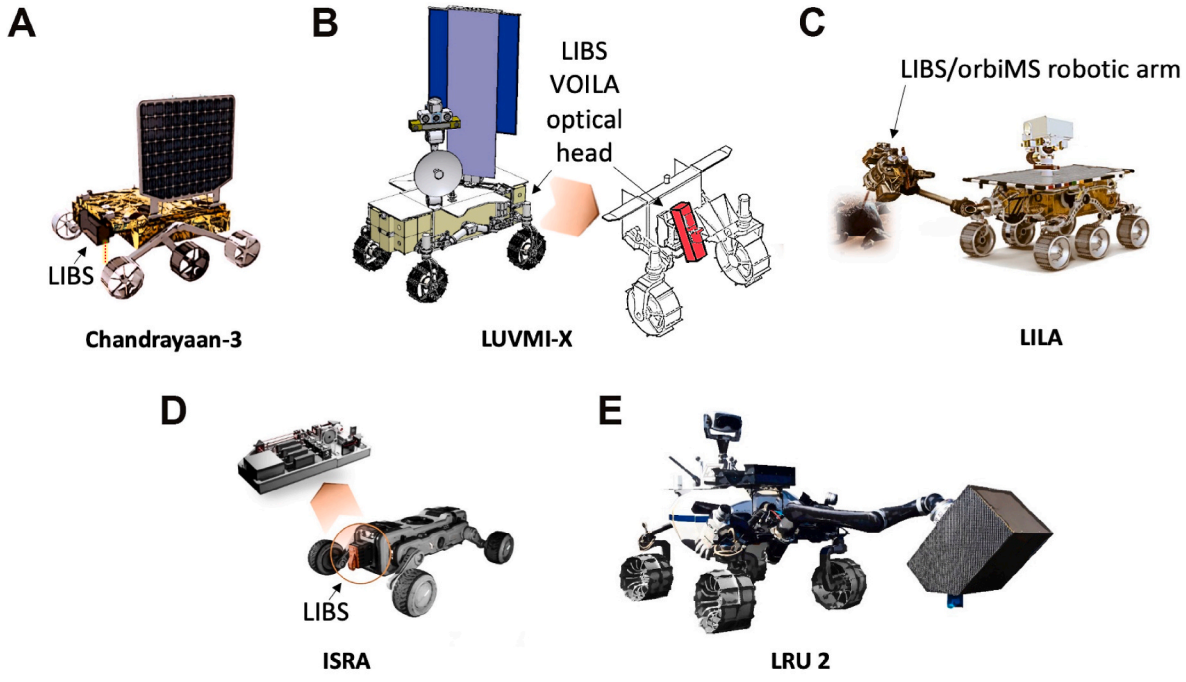

Fig. 5. (A) A schematic of the Chandrayaan-3's Pragyan rover. **(B)** A concept of the LUVMI-X rover carrying the VOILA LIBS instrument. **(C)** A schematic representation of LILA, the next-generation moon rover designed to apply technologies developed in the Czech SLAVIA project to future lunar missions. **(D)** A concept of the ISRA payload on the generic rover, a commercial LIBS instrument by Lightigo Space. Note that the rovers are not presented on a unified scale. **(E)** Lightweight Rover Unit by DLR.

measurements. Preliminary results indicated the presence of sulfur, among other elements. Currently idling mission aimed to develop another prototype LIBS payload, the so-called VOILA (Volatiles Identification by Laser Analysis) instrument implemented on the LUVMI-X (Lunar Volatiles Mobile Instrumentation-Extended) rover [86,89].

Most recently, the interest in LIBS and its use in various segments of ISRU [90] (mainly prospecting) on the Moon is reflected in the proposition of LIBS instruments that could be commercially available. This is a promising prospect for future development of space-grade LIBS systems (e.g., the concept of a LIBS payload by Lightigo Space). Moreover, the Lightweight Rover Unit (LRU) by the German Aerospace Center (DLR) was demonstrated to work successfully with the DLR ARCHES LIBS module during an analog space mission at Mt. Etna, Sicily [91]. Meantime, inspired by the advancements in our research project, we proposed the design and development of LILA, a pioneering moon rover tailored for future lunar explorations. LILA incorporates Laser Ablation (high--resolution) Mass Spectrometry (LAMS) and LIBS. As depicted in Fig. 5, it embodies cutting-edge technologies derived from the Czech SLAVIA (Space Laboratory for Advanced Variable Instruments and Applications) CubeSat mission, enhancing lunar exploration capabilities. Thus, the rover promises to advance our understanding of lunar environments significantly. It has potential applications in comprehensively analyzing the lunar surface, providing data on the bulk elemental composition, mineralogy, rock composition, and detection of trace elements, isotopes, molecules, and volatiles through a combination of LIBS and LAMS.

Despite the recent in-situ utilization of LIBS on the Moon, several works already explored its potential for lunar applications in simulated conditions. Additionally, general studies on low-pressure LIBS are particularly relevant, given the Moon's lack of atmospheric pressure. The absence of ambient conditions (gas and pressure) significantly affects plasma formation and, consequently, its spectral emission, presenting new challenges compared to Earth's or Mars's atmospheres. In the case of LIBS analysis under high-vacuum conditions, it was found that once the vacuum reaches pressures lower than 10^{-3} mbar ($\approx$ 100 mPa or 0.75 $\times$ 10^{-3} Torr) the plasma is no longer confined by the surrounding atmosphere and can be considered as a freely expanding plasma [1]. Thus, any further decrease in pressure (getting to a higher vacuum) will not significantly affect the quality of LIBS spectra and in turn its analytical performance. It is typically hypothesized that the LIBS plasma in experimental conditions at 10^{-4} mbar ($\approx$ 10 mPa or 0.75 $\times$ 10^{-4} Torr) will behave similarly to a real LIBS plasma on the surface of the Moon, where the pressure is significantly lower.

The feasibility of LIBS for the Moon was first demonstrated in simulated conditions with pressures as low as 5 mTorr ($\approx$ 666 mPa or 7 $\times$ 10^{-3} mbar) [37]. However, a significant signal decrease for pressures below 1 Torr ($\approx$ 133 Pa or 1.33 mbar) led to increased detection limits. According to Ref. [92], 50 mTorr ($\approx$ 6.7 Pa or 0.07 mbar) served as an entry point to simulate lunar conditions and led to reduced matrix effects compared to Earth and Mars atmospheres. The paper also focuses on the way of collection of optical emission spectra which is one of the most critical methodological steps in the case of free-expanding laser--induced plasmas. Follow-up work in pressures below 0.75 mTorr ($\approx$ 100 mPa or 10^{-3} mbar) estimated the limits of detection (LOD) for major elements in lunar regoliths were typically <1 wt% [93]. Recently, the detection of hydrogen was assessed in simulated conditions (10^{-2} Pa, $\approx$ 10^{-4} mbar or 10^{-4} Torr) [94]. To create a calibration curve, basalts and feldspar samples were mixed with hydroxyls into H-rich samples. The results showed LODs below 0.4 wt% for H_2O. Finally, a strategy with a continuous-wave laser was adopted in order to heat up the sample prior to ablation. This led to distinguishing the provenance of H between frozen water and hydroxyl structures. The sample preheating evaporates water from the sample, thus decreasing the H signal response. On the opposite, the preheating has no significant effect on H in hydroxyl molecules.

In contrast to conventional atmospheric LIBS, simulated lunar conditions have proven beneficial for detecting vacuum-UV spectral lines [95]. This was demonstrated for sulfur lines (LOD below 5 at%), which are notoriously difficult to detect with conventional LIBS. Notably, calibration curves for sulfur exhibited no saturation, which confirmed the suppression of matrix effects at low pressures. Further insights for plasma dynamics in low pressures were provided by modeling [96]; introduced a numerical model employing a 1D thermal conductivity equation and hydrodynamic simulations. Thus, the research activity in VUV LIBS and namely the understanding of the behavior of LIP under vacuum conditions can guide further development of LIBS for lunar exploration.

5. LIBS on asteroids: prospecting and analyzing meteorites

Our current understanding of asteroids and comets derives largely from telescopic studies [97] and the examination of meteorites [98,99], micrometeorites, and interplanetary dust [100]. These investigations reveal their vast chemical and physical diversity, shaped by complex solar system evolution and possibly the capture of interstellar objects [101]. With over 523,000 asteroids identified [102], the direct, systematic exploration of a statistically significant sample by a spacecraft remains currently unfeasible due to technological and logistical constraints [103]. Despite the challenges, the prospect of space resource utilization makes systematic exploration of asteroids highly attractive. Alternative strategies such as remote sensing via a fleet of flyby probes or landers present viable approaches for extensive and statistically representative data collection [104].

Despite the scientific community's increasing interest in employing LIBS for missions targeting such environments [105], to date, no specific asteroid mission utilizing LIBS has been proposed or undertaken. The unique challenges posed by asteroid exploration, including microgravity conditions, the necessity for precise targeting mechanisms, and varying distances from Earth, necessitate tailored adaptations of LIBS technology to meet these demands.

Remote sensing through astronomical telescopes offers a cost-effective alternative, albeit with limitations in detecting physical and optical properties and in establishing direct correlations between elemental compositions and spectral data [106–109]. Spectroscopy primarily detects silicates rather than economically valuable elements, though high radar reflectivity has indicated the presence of enstatite and FeNi alloys on asteroids like 216-Kleopatra [110]. In-depth analysis has also been achieved through missions of several spacecraft to asteroids, which, despite the significant energy and time required, yield very comprehensive data [111]. Missions like the Galileo spacecraft's flybys of 951 Gaspra and 243 Ida [112], and the NEAR-Shoemaker's visit to 433 Eros [113] have provided detailed insights into asteroid composition. Similarly, the OSIRIS-Rex mission to 101955 Bennu and Hayabusa2's mission to 162173 Ryugu have returned samples for Earth-based analysis [114–116]. These missions underscore the potential for targeted exploration and mining, though the economic viability and technological challenges remain considerable.

The LIBS technique, notably deployed by the Chandrayaan-3 lunar rover [87], has demonstrated its potential for elemental analysis on airless planetary bodies, highlighting its relevance for future asteroid exploration missions. The future LIBS system applicable for asteroid exploration will likely benefit from two leading interplanetary matter research approaches applied in contemporary science: (a) remote spectral analysis of meteors provides insight into the elemental composition of interplanetary matter. This occurs when meteoroids enter the Earth's atmosphere and create meteor plasma, where the characteristic emission of elements present in the meteoroid body can be detected by spectral analysis of radiated light. Similar to classical LIBS, the elemental abundances can be determined [119–121]; and (b) lab-based analysis of meteorites combined with other techniques enabling reference quantification of elemental abundances [15,122].

LIBS has been extensively used to analyze meteorites in the laboratory, yielding valuable data on their elemental and isotopic composition.

However, the laboratory examination of meteorite samples with a wide range of techniques, not only LIBS, offers valuable insight into the composition of interplanetary matter. The most problematic issue is tracking the original source of a particular meteorite, which is almost completely unknown. Based on mineralogy and isotopic composition, some meteorite find can be associated with Mars or the Moon [123,124]. However, for asteroids, precise orbital trajectory and their original source, was calculated for only about 30 cases [125].

Conversely, in most cases of meteor observations, the meteoroid is completely evaporated and lost in the atmosphere due to harsh conditions such as high-temperature ablation or aerodynamic and mechanical stress during atmospheric descent. The first semi-quantitative LIBS analysis of a meteorite sample was carried out by A. Petrakiev in 1970 [126]. Since then, LIBS has repeatedly been used for the bulk elemental analysis of large samples of meteorites [119,122,127–132]. These studies mainly point to the versatility and speed of LIBS in examining any meteorite sample without cutting or other preparation and the ability to detect major and, in a limited way, also trace elements which are essential for understanding the processes that formed these extraterrestrial materials.

Another interesting approach is represented by the laser ablation simulation of meteor spectra in the laboratory. This idea was originally proposed by William J. Rae and Abe Hertzberg from the US Cornell Aeronautical Laboratory in 1964 [133]. In the early 1970s, Hapke et al. [134] employed laser ablation in the first simulation of impact evaporation, and Pirri et al. [135] pioneered the first fundamental description of laser light interaction with targets. Since then, this approach has expanded significantly in a wide range of studies focused on the experimental exploration of meteor physics and chemistry using tabletop lasers as well as large high-power laser infrastructures [121, 136]. These experiments focused on meteor plasma physics and chemistry, as well as ground-based observations, are crucial intermediate steps towards systematic asteroid belt exploration and resource prospection by space missions. Spaceborne observation of meteors is dedicated to the development of corresponding technologies [104,121].

Overall, LIBS has proven to be a powerful tool for the analysis of meteorites, providing insights into their composition, formation, and history. The application of LIBS to meteorite studies not only enhances our understanding of these extraterrestrial materials but also demonstrates the technique's potential for future asteroid exploration missions, where in-situ analysis of surface and subsurface materials will be crucial for resource identification and utilization. These missions to near-Earth or Main Belt asteroids will benefit from both meteor spectroscopy and lab-based LIBS analysis of meteorites. The asteroid-bound missions could use LIBS payloads to leverage its on-site chemical analysis capabilities and ability to access subsurface materials by removing surface layers [104]. For instance, a recent study [94] has put forth a promising approach for the in-situ analysis of hydrogen-bearing compounds using LIBS, indicating the technique's high sensitivity for detecting hydrogen in lunar soils. Additionally, the potential for using LIBS or conducting spectral surveys of material clouds evaporated by a laser during flyby missions has been explored [137,138]. However, these applications, especially those necessitating high-power lasers, highlight the imperative for substantial advancements in space technology. These advancements include enhancements in targeting accuracy, optical systems, and power supply management, which are crucial for fully leveraging LIBS capabilities in asteroid missions [137]. A notable instance of such a conceptual large-scale mission is the Directed Energy System for Targeting of Asteroids and Exploration (DE-STAR) [117], depicted in Fig. 6 (A). Additionally, Panel B showcases an example spectrum of a terawatt-class meteorite specimen's ablation plasma [118].

6. Data processing for LIBS space applications

In this section, we focus on the advancements and challenges in LIBS data processing for space applications, primarily in the context of Martian exploration. A significant portion of the research has been directed towards quantifying the elemental constituents of geological samples, especially the simulation of Martian regoliths (their simulants, to be precise) and an array of rock types and soil simulants. Alongside quantification, other key areas of exploration include classification, clustering, and implementing transfer learning and spectral libraries. An overview of these data processing techniques and their applications can be found in Table 2.

The primary challenges in this domain include addressing data variability due to environmental changes and instrumental discrepancies (*e.g.*, caused by rapid temperature changes), which often result in spectral drift. Moreover, the target materials, *i.e.*, geological targets, exhibit significant variances in physical and chemical properties. Namely, the absorption efficiency of the ablation laser pulse is affected by the opacity of the material, while the ablation rate depends on the material's consistency [139] or the material grain size [140].

Recent progress in the field is highlighted by improved calibration methods, the adoption of sophisticated machine learning algorithms, and innovative approaches like adaptive spectral drift correction and transfer learning. These developments have markedly enhanced the precision and reliability of LIBS data analysis, a critical aspect of comprehending the composition and geological properties of Martian samples. An equally important research direction is exploring the impact of the amount of data used for constructing calibration models for either "big data" statistics or dimensionality reduction approaches. Namely, concerning the former, the openly available ChemCam and SuperCam calibration datasets already consist of spectra from over 400 and 330 targets, respectively [139]. Several follow-up studies have been performed using these datasets since their publication, highlighting the potential benefits of large open-access datasets in the spectroscopic community.

Below, we first present the most common data processing pipelines

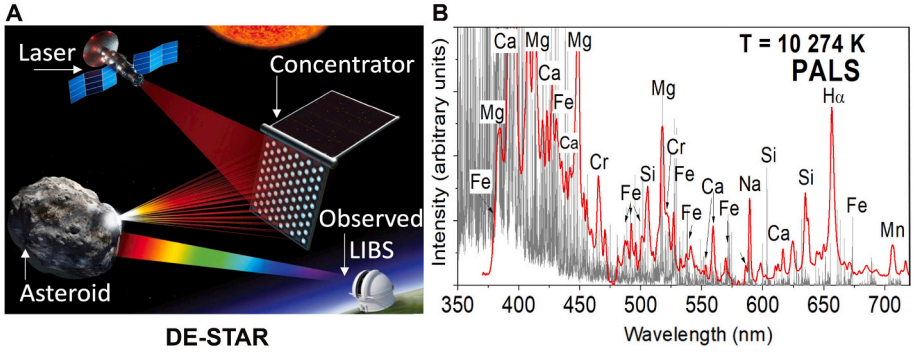

Fig. 6. **(A)** Conceptual large-scale mission of the Directed Energy System for Targeting of Asteroids and Exploration, DE-STAR, [117]. **(B)** Example of a chondritic meteorite LIBS performed by high-power terawatt-class laser. The data are newly recompiled from the original study [118].

Table 2
Overview of data processing for LIBS space applications.

Methods	Targets	Goal & Analytes	Evaluation Metric Dataset size	Instrumentation Note	Ref.
OLS, PLS,LASSO, ridge regression, elastic net, Orthogonal Matching Pursuit, SVR, Random forest, Grad Boosted regression, Local Elastic Net, Blended Submodels	Martian regolith simulants SuperCam calibration dataset	**Quantification:** SiO2, TiO2,Al2O3,FeOT, MgO, CaO, Na2O, K2O	RMSEP *334 Targets*	SuperCam	[139]
Elastic net	Martian regolith simulants ChemCam calibration dataset	**Quantification:** SiO2, TiO2, Al2O3,FeOT, MgO, CaO, Na2O, K2O	RMSEP *408 Targets*	ChemCam	[155]
CNN, ensemble CNNs, PLSR, extreme learning machines	Martian regolith simulants	**Quantification:** SiO2, Al2O3, K2O	RMSECV, RMSEP, $\mathbb{R}^2$, relative error *408 Targets*	ChemCam	[153]
PLSR, SIMCA, PLS-DA	Igneous and highly metamorphosed rock samples	**Quantification:** SiO2, TiO2, Al2O3, FeOT, MgO, CaO, Na2O, K2O	Classification accuracy *18 Targets*	Early ChemCam design	[156]
PLSR, univariate regression	Martian regolith simulants (doped)	**Quantification:** SiO2, TiO2, Al2O3, FeOT, MgO, CaO, Na2O, K2O, Ni, Mn,Zn, Cr, Co	RMSE-CV *452 Targets*	Laboratory-based ChemCam-analog	[157]
Univariate regression, PCR, PLSR, Ridge, LASSO, elastic net, MLP	Forsterite and olivine targets	**Quantification:** Mg2SiO4, Fe2SiO4	$\mathbb{R}^2$, MAE, RMSE *14 Targets*	MarSCoDe	[158]
CNN, logistic regression, SVM, LDA	Pelletized rock powders	**Classification based on the composition:** Si,Fe, Mg, Al, Ca, K	Classification accuracy, Brier score *12 Targets*	MarSCoDe	[159]
PLS	Martian regolith simulants	**Quantification:** SiO2, TiO2, Al2O3, FeOT, MgO, CaO, Na2O, K2O	RMSE *55 Targets*	MarSCoDe ChemCam	[160]
PLSR, ICA, Multivariate Oxide Composition (MOC), ICA	Martian regolith simulants	**Quantification:** SiO2, TiO2, Al2O3, FeOT, MgO, CaO, Na2O,K2O	RMSE *408 Targets*	ChemCam	[141]
NA	Si wafer, Si sillicon grains polished quartz crystal, pure metal targets (Al, Co, Fe, Ni, Ti)	**Basic research:** Si, C emission line standardization	NA $\geq$ *20 Targets*	DLR LIBS system	[161]
ICA and multivariate linear regression	Martian regolith simulants	**Quantification:** SiO2, TiO2, Al2O3, FeOT, MgO, CaO, Na2O, K2O	$\mathbb{R}^2$, RMSE *8 Targets*	Laboratory-based ChemCam-analog	[140]
PLSR, kNN	Pelletized rock powders	**Quantification:** Si, Al, Fe, Ca Mg	RMSE *49 Targets*	Commercial laboratory-based systems	[162]
PLSR	Chemcam calibration targets	**Quantification and Calibration transfer:** SiO2, TiO2, Al2O3, FeOT, MgO, CaO, Na2O, K2O	RMSEP, Intensity error *408 Targets*	ChemCam	[163]
Probabilistic Major Element Composition (PMEC), natural gradient boosting probabilistic prediction (NGBoost)	Martian regolith simulants	**Quantification:** SiO2, TiO2, Al2O3, Fe2O3T, MgO, CaO, Na2O, K2O	RMSE *93 Targets*	MarSCoDe	[164]
MLP	Nautral rocks	**Quantification:** Li, Rb, Sr, Ba, SiO2, Al2O3, Fe2O3, K2O, Na2O, CaO, MgO	$\mathbb{R}^2$, RMSE *27 Targets*	Custom laboratory system	[151]
PLS, LASSO	Pelletized rock powders	**Quantification:** Si, Fe, Mg, K, Na, Ti, Ca, Al, O, H, C	RMSE *316 Targets*	SDU-LIBS MarSCoDe	[143]
CNN, MLP, SVM, Logistic regression, LDA	Standard reference materials rocks, soils, sediments and ores	**Classification:** rock type	Classification accuracy *39 Targets*	MarSCoDe duplicate	[165]
PLSR sub-models	Pelletized rock powders	**Quantification:** TiO2, Al2O3, Fe2O3, MnO, P2O5, and trace elepement dopants.	RMSE *2990 Targets*	Laboratory-based ChemCam-analog	[152]
PLSR	Pelletized rock powders	**Quantification:** SiO2, Na2O, MnO, Li, Ni, Pb, Rb, Sr, Zn	LOQ *3001 Targets*	Laboratory-based ChemCam-analog	[166]
Siamesse CNN	Martian regolith simulants ChemCam calibration dataset	**Automized preprocessing**	RMSE, Mutual information *408 Targets*	ChemCam	[154]
MOC, NMF, K-means, random forest classifier	Martian in-situ observations	**Classification:** rock type	Classification confidence *2300 Targets*	ChemCam	[167]

(*continued on next page*)

Table 2 (*continued*)

Methods	Targets	Goal & Analytes	Evaluation Metric Dataset size	Instrumentation Note	Ref.
MLP	Pelletized, raw, polished rocks	**Quantification:** SiO2, Na2O, K2O	RMSE *20 Targets*	Laboratory system	[144]
PLS, LASSO, mixture models, univariate regerssion, OLS, ridge Regression, elastic net, Orthogonal Matching Pursuit (OMP), Automatic Relevance Determination (ARD), Bayesian Ridge Regression (BRR)	Manganese-bearing rock, mineral, metal ore, and synthetic standards	**Quantification:** Mn	RMSEP, precision LOD, LOQ *523 Targets*	ChemCam testbed	[147]
CNN	ChemCam calibration dataset and in-situ data	**Quantification:** SiO2, TiO2, Al2O3, FeO, MnO, MgO, CaO, Na2O, K2O	Qualitative and quantitative chemical content (QQCC), RMSE *408 Targets*	ChemCam	[142]
Linear Mixture Model (linear mixture of sub-models)	Pelletized rock powders	**Quantification:** SiO2, TiO2, Al2O3, FeO, MnO, MgO, CaO, Na2O, K2O	RMSE *10 Targets*	ChemCam	[148]
PLSR, SVM (for submodel classification)	Martian regolith simulants ChemCam calibration dataset)	**Quantification:** SiO2, TiO2, Al2O3,FeO, MnO, MgO, CaO, Na2O, K2O	RMSE, $\mathbb{R}^2$ *408 Targets*	ChemCam	[168]
PLSR	Pelletizedrock powders of eight matrices doped with 25 trace and minor elements	**Quantification:** 65 elements	RMSE, error of the calibration (RMSE-C), error of cross-validation (RMSE-CV), and the error of prediction (RMSEP) *2959 Targets*	Laboratory-based ChemCam-analog	[169]
PLSR blended sub-models	Martian regolith simulants ChemCam calibration dataset	**Quantification:** SiO2, TiO2, AL2O3, FeOT, MgO, CaO, Na2O, K2O	RMSE *408 Targets*	ChemCam	[170]
CNN, SVM, PLSR	Martian regolith simulant ChemCam calibration dataset	**Quantification:** SiO2, TiO2, AL2O3FeOT, MgO, CaO, Na2O, K2O	RMSE *376 Targets*	ChemCam	[171]
Univariate regression	Pelletized rock powders	**Quantification:** Al2O3, CaO, Fe2O3,K2O, MgO, MnO, Na2O,P2O5, SiO2, TiO2, Ba, Cr, Cu, H2O, Li, Ni,Pb, S, Zn	RMSE, LOD, $\mathbb{R}^2$ *2843 Targets*	Commercial handheld LIBS	[172]
PLS	Salt/basalt mixtures, sulfates	**Qualitative:** clustering	RMSE, cluster distances *25 Targets*	Custom laboratory system	[173]
CNN, MLP, PLS	Standard reference materials rocks, soils, sediments and ores	**Quantification:** SiO2, Al2O3, Fe2O3, CaO, MgO, K2O, Na2O, FeO.	RMSE, relative error (RE) *23 Targets*	MarSCoDe	[145]
Univariate and multivariate regression, LASSO, PLS	Pelletized rock powders	**Quantification:** Li, B, CO2, S	– $\geq$ *2900 Targets*	Laboratory-based ChemCam-analog	[174]
Univariate and multivariate regression, LASSO, PLS	rock and mineral standards	**Quantification:** H	LOO-RMSE-CV *198 Targets*	Laboratory-based ChemCam-analog	[149]
NA	In-situ Mars targets	**Classification**: rock and mineral type	wt.% $\geq$ *1000 Targets*	ChemCam	[52]
NA	Martian regolith simulants MarSCoDe calibration dataset	**Emission line identification:** Ti, Si, Al, Fe,Mg, P, Ca, Na, K, O, C, H, S	NA *33 Targets*	MarSCoDe	[11]
PLS regression	Pelletized rock powders doped with hydroxyls	**Quantification:** H	RMSE, Q^2, MedRE *99 Targets*	Custom laboratory system	[94]

used for quantitative analysis. Then, we briefly list the methods used for qualitative analysis (both supervised – classification – and unsupervised – clustering). Last, we give an overview of the approaches proposed to address the data shift that inherently plagues the applicability of LIBS in space research.

6.1. Preprocessing

Almost universally, the spectra are pre-processed in 3 steps: denoising, baseline correction, and wavelength [141], and intensity calibration (the latter is also commonly referred to as instrumental response calibration [142]. Denoising is commonly carried out using wavelet decomposition using Daubechies Wavelets [143]. Nevertheless, these wavelets tend to introduce artefacts. Consequently, an alternative bi-orthogonal wavelet family is commonly used [139]. Baseline correction is done either using wavelet decomposition (although with different wavelet parameters than those used for denoising, such as cubic-spline [144], or by polynomial and spline fitting [143]. Lastly, wavelength calibration is generally done using the spectra of a standard material such as Ti [139], although continuous automated approaches, such as adaptive spectral drift correction (ASDC) have also been proposed [78].

In some cases, wavelength masking is employed, which omits low-quality spectral regions from further analysis [145]. The quality of the spectral regions is commonly quantified by the signal-to-noise ratio (SNR). Another important but less frequently reported step is outlier

detection (and potential filtering). Outlier detection is frequently performed via isolation forests [139,146,147], local outlier factor analysis [139,147], or partial least squares (PLSR) residual analysis combined with Hotelling's T2 plots [141].

Scaling to unit sum [144], or unit maximum [148] intensity is generally applied as a post-calibration procedure which facilitates numerical or statistical data mining. Other than the area under the curve and global maximum, other, more specific internal standards have also been used for normalization [149]. The shot-to-shot variance of LIBS is commonly addressed (as a first step) by applying spectrum-wise standardization (standard normal variance, SNV) [144], or various bootstrapping [150] variants [151], where the latter is also a common tool for simple dataset augmentation [152,153]. Considering the variety of preprocessing techniques, there have been several attempts to automate the process with the aim of reducing the need for domain expertise and extensive hyperparameter tuning. Notable approaches include using Siamese neural networks for end-to-end preprocessing [154].

The last preprocessing step frequently applied is feature extraction and/or dimensionality reduction. The most straightforward approach is to apply a peak finding algorithm and manually identify the emission lines found [158]. Subsequently, emission lines of interest can be selected based on the target application. This peak finding approach can be generally improved by peak fitting to enhance emission line intensity estimation and to reduce noise and self-absorption effects. Two common peak profiles are the Lorentzian [161] and Voigt [174] profiles, as is well established in the LIBS literature. Nevertheless, peak fitting can be computationally demanding and requires a good guess of the initial peak parameters. A simpler but potentially equally beneficial approach is peak binning [139], which aggregates intensities between two local minima, hence approximating the line intensity.

Among automated approaches to dimensionality reduction, principal component analysis (PCA) is a frequent choice [173], which is in line with the overall ambivalence of PCA in LIBS [175]. Nevertheless, PCA has been outperformed by independent component analysis (ICA) [141], which was found to work especially well with linear models [148]. The list of matrix decomposition-based dimensionality reduction would be incomplete without mentioning non-negative matrix factorization (NMF) [167], which offers a clear benefit over PCA and ICA of working with physically meaningful non-negative feature weights. Apart from decomposition techniques, iterative feature selection methods have also been proposed, such as the SelectBest algorithm, which finds the spectral channels with the highest correlation with the target analyte [151]. Interestingly, these channels are often not the emission line centres but pixels approaching their tail region.

6.2. Quantification

The primary focus of quantitative LIBS analysis in the context of space exploration is the quantification of such principal geochemical analytes as SiO_2, TiO_2, Al_2O_3, $FeTiO_3$, MgO, CaO, Na_2O, or K_2O [155–157,160]. In addition, several studies have addressed the quantification of minor or trace elements, such as B, Ba, C, Ce, Co, Cr, Cs, Cu, Ga, La, Li, Mo, Nb, Ni, Pb, Rb, S, Sc, Se, Sn, Sr, Y, Zn, and Zr. These are generally studied using soil doped targets [152]. Lastly, quantifying H content in soil targets (with the overall aim of quantifying water content) is another notable research direction [94,149]. In most cases, the model's performance is evaluated in terms of mean squared error (MSE), root MSE (RMSE), or R2 [153,158]. Less commonly, mean absolute error is applied [158]. In some cases, estimated limit-of-detection (LOD) [147], or limit-of-quantification (LOQ) [166] are also reported (including multivariate models, which are not commonly found in the literature).

Quantitative studies employ both univariate [147,158,172], and multivariate [170,171] models. Almost universally, multivariate approaches were shown to outperform univariate ones [157]. Most works employ "traditional" machine learning models, i.e., not including deep learning. Namely, linear models such as ordinary least squares and partial least squares regression models are especially popular due to their straightforward interpretability [139,147,158,168,169]. Considering the number of predictors present in LIBS spectra (the number of resolved wavelengths), these models are generally regularized using either a sum-of-squares term (ridge regression) [139,158], sum-of-absolute-values term (lasso regression) [143,147,149,174], or a mixture of the two (elastic net regression) [139,158] to avoid potential overfitting.

A common limitation that linear models face in the context of geological quantitative analysis is the wide concentration range of most of the analytes of interest. Consequently, most analyses face the challenges presented by non-linear curves of growth. To address this challenge using a linear model, the so-called sub-model approach was introduced [139]. The sub-model approach uses several regression models, each targeting a limited portion of the considered complete concentration range of the analyte where it yields superior accuracy as compared to a so-called global model covering the entire range [139]. This sub-model approach has since been iteratively improved by optimizing the sub-models weights and the overall merging of the individual model outputs [147,152]. Among the proposed improvements, the sub-model weight optimization using a particle swarm optimization procedure is especially noteworthy [170].

An overall distinct direction is nonetheless marked by the increasingly popular non-linear regression models. While initial studies reported the comparison between the usual linear models and non-linear alternatives, such as random forests and gradient boostingmodels (in general decision tree ensembles) [139,147,164], the comparisons did not include artificial neural networks and deep learning models, which dominated other fields such as computer vision and natural language processing. Nevertheless, recent efforts have been made to supplement these results by exploring the validity of deep learning. Specifically, the elemental composition of rock samples has been quantified using multilayer perceptrons (MLPs, also known as dense or fully connected neural networks [144,145,151,176,177]. Neural networks, namely convolutional neural networks, have been applied to more extensive datasets as well, such as the ChemCam extended calibration dataset [142], where they were shown to outperform PLSR and support vector machine regression models [171].

6.3. Classification

While classification in this context is arguably less challenging than precise quantification, it does present several issues that need to be addressed. Key among these is the high similarity between the class compositions and a limited number of standards for constructing robust models. Various approaches have been employed in the literature, ranging from simple linear models to the recent adoption of deep learning models.

In addition to standard preprocessing steps, an essential task is the creation of ground truth class labels. The process of assigning these labels is highly specific to the problem, often based on the selected ranges of composition [168] or additional information about the samples [156,165]. The preprocessing relevant to the classification usually contains spectral drift correction and scaling to unit maximum intensity. These steps are critical in enhancing the model's ability to distinguish between spectral features, thereby improving classification accuracy.

The soft independent modelling of class analogy (SIMCA) was used to classify spectra in the first pre-ChemCam study [156,178]. Subsequently, more extensive datasets, like the in-situ ChemCam data, were classified by random forests (RF) after the feature selection by non-negative matrix factorization (NMF) and repeated k-means clustering for obtaining class labels [167].

Convolutional neural networks (CNNs) outperformed traditional models such as logistic regression, support vector machines (SVMs), and linear discriminant analysis (LDA) in the classification of spectra from a

laboratory copy of Mars Surface Composition Detector(MarSCoDe), even with a limited number of training samples [159]. Similar outcomes were observed with spectra measured at varying laser-target distances [165].

In some studies, classification was a part of more general pipelines, such as enhancing quantification processes. For instance, SVMs with radial basis function kernels have been used to classify spectra into categories, which then informed the construction of distinct PLSR models, improving the RMSE on the ChemCam calibration dataset [168]. K-nearest neighbours (KNN) model was also employed for validating spectra transfer based on dynamic time warping (DTW, see details below) [162].

Given the overlapping nature of tasks and challenges in these studies, there is a clear need to establish benchmarks and baseline methods for material classification in space applications. This would streamline future research efforts and help distinguish truly innovative work in the field.

6.4. *Transfer learning*

Transfer learning is a uniquely crucial part of applying LIBS in space applications: The calibration of LIBS instruments can only be performed on Earth in stable laboratory settings simulating the target planet's atmosphere. On the contrary, the instrument collecting the in-situ data is deployed in an ever-changing environment. Hence, continuous efforts are being made to improve the accuracy of the models when applied to in-situ data. These efforts to adapt the calibration models to data collected from changing environments are referred to as calibration library transfer (or calibration transfer for short). The first attempt reported to perform calibration transfer from a source (e.g., laboratory) system to a target (e.g., in-situ Mars) system simply used the ratio of the mean spectra of a set of selected calibration standards measured under both simulated and real Martian conditions [139,141,179]. This approach is also sometimes referred to as piecewise direct standardization (PDS) [162]. As an improvement upon PDS, dynamic time warping (DTW) was adapted from the field of signal processing [162]. More complex approaches relying on deep learning have also been proposed. Namely, replacing the simple ratio between the source and target data, a transformation was constructed via training a (deep) extreme learning machine [163], MLPs [180], or variational autoencoders (VAE) [181]. In particular, VAEs offer extensive flexibility for data augmentation and transfer learning [181].

An alternative approach is to employ data-based transfer learning. Therein, instead of finding a transformation between the source and target datasets, the spectral channels are filtered so that only those robust against the changing measurement conditions are maintained [151]. Nevertheless, this approach has been so far limited to calibration transfer between distinct target matrices, such as pelletized or raw rock samples [151].

7. Modelling of laser-induced plasmas under atmospheric conditions of celestial bodies

An adequate model of laser-induced plasma is highly desirable for the conditions expected in space missions: *e.g.*, vacuum (as on the Moon), low pressure CO_2 atmosphere (as on Mars), high pressure CO_2 atmosphere (as on Venus), and a large range of ambient temperatures and different types of materials analyzed. Such a model can help find optimal experimental parameters for laser ablation under simulated planetary conditions and to obtain both qualitative and quantitative information about the samples under study. These parameters can then be found at low cost without performing tedious and time-consuming optimization experiments.

Since optical spectra are the main channel of information in LIBS, the quality and unambiguous interpretation of these spectra are of paramount importance to obtain accurate information about the materials exposed to the laser. The spectra however intrinsically depend on a large number of parameters, such as the energy and duration of the pulsed laser radiation, laser wavelength, surface properties, material and surrounding gas composition, ambient pressure, temperature, etc. These parameters intertwine in complex ways, and much effort has been made to understand their role through modeling and computer simulation of laser-induced plasma. Over the past two decades, a large amount of literature and several reviews have been published on this topic [183–186].

In general, ablation plasma is modeled using three theoretical approaches.

i analytical [187–191],
ii hydrodynamic [182,192–199], and
iii Monte Carlo [200,201].

During ablation into vacuum, as in the case of lunar exploration, it can be assumed that ablated particles directly undergo adiabatic expansion, for which analytical solutions exist [187–190]. This is the simplest case of simulation in which the hydrodynamic equations are solved under the assumption of local thermodynamic equilibrium, which assumes a collisional interior of the ablation plasma plume. Anisimov et al. [187] obtained a simple analytical solution for the range of parameters characteristic of LIBS in vacuum. Cools et al. [188]solved the problem of unstable adiabatic vacuum expansion considering transport through the Knudsen layer with specific boundary conditions. Gornushkin et al. solved the equations of hydrodynamics and radiation transfer for spherical [189], and elliptical [190]vacuum ablation to obtain the evolution of plasma temperature, plasma particle concentration and plasma spectrum. It is noteworthy that the flow equations describing vacuum ablation remain valid only until the density reaches a critical value; beyond this value, particles abruptly go into free flight [191]. For ablation into ambient gas, as would be the case for exploring Mars with its low-pressure CO_2 atmosphere, an analytical solution is difficult to obtain due to the difficulty of processing the shock discontinuity generated by the supersonic expanding plasma plume. Despite attempts to obtain analytical solutions [192,193], numerical solutions, in this case, seem to be more adequate. The rigorous fluid dynamics (FD) approach typically involves solving the three-dimensional compressible Navier–Stokes equations for a multicomponent gas, including the effects of mass and forced diffusion, as well as thermal conductivity and viscosity. Many models have been proposed using FD numerical simulations. Ho et al. [194], and Gusarov et al. [195] developed the models which combined one-dimensional surface evaporation and two-dimensional FD equations describing the plasma plume. Since plasma chemistry has a significant impact on both plasma dynamics and emission spectra, chemical reactions have been included in later FD plasma models. Babushok et al. [196] developed a numerical algorithm for solving two-dimensional Navier–Stokes equations coupled with finite-rate chemical kinetics and applied it to study the influence of chemical reactions on flow dynamics. Casavola et al. used a two-dimensional [198] FD model to study the ablation of titanium into nitrogen, in which LTE was assumed to be valid for ionization and chemical dissociation processes. Shabanov et al. [198,199], and Gornushkin et al. [182,200], finally, developed numerical FD algorithms that included ionization and chemical reactions to calculate the ablation of various materials into air, N_2, Ar, and other reactive and inert atmospheres. For example, the model was applied to estimate the plasma chemical composition and rate of reverse deposition of titanium oxides onto the titanium surface during ablation of titanium into atmospheric air [182]. These results are illustrated in Fig. 7.

The third group of models, Monte Carlo, is used for plasmas with strong gradients, where the velocity distribution of ablated particles deviates from Maxwellian. In addition, they describe the mixing of ablated and surrounding gas particles and sorption/desorption on solid surfaces. Urbassek et al. [201] developed a Monte Carlo model for

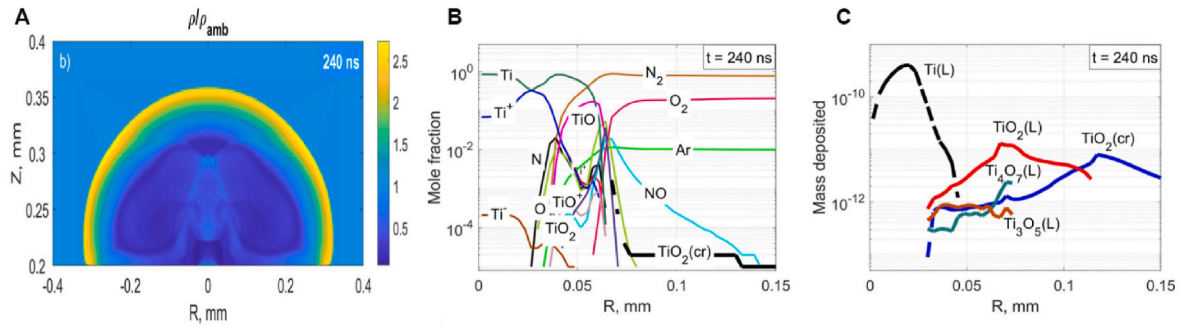

Fig. 7. Results of FD-chemical calculation of titanium ablation into atmospheric air, **(A)** plasma density profile after 240 ns of evolution of the plasma plume (the separation of the shock from the surface of the plume is clearly visible), **(B)** the equilibrium chemical composition of the plasma plume, including both gaseous and condensed species, **(C)** condensed species accumulated on the surface during 240 ns of plasma evolution. Adapted with the permission from Ref. [182].

vacuum ablation, considering collisions between particles and assuming a thermal desorption mechanism. Itina et al. [203] combined a continuum FD approach for the first stage of plume expansion with a direct Monte Carlo simulation of the ablated plume into the background gas at a later stage. Hansen et al. [204] iteratively fitted a steady-state two--zone LTE plasma model to LIBS spectra obtained in a simulated Martian atmosphere, allowing elemental concentrations to be estimated with an accuracy of about 25 %. Remarkably, the method requires no calibration and can be applied to any sample composed of elements with available atomic data. Light collection by a suitable optical system is sometimes part of a plasma model to optimize the collection geometry as well. As an example, a combination of an expanding plasma plume model with a geometric plasma radiation collection model was proposed by Shabanov et al. [205] to calculate the emission spectra of an ellipsoidal plasma collected by a lens or optical fibre.

8. Hyphenated LIBS methods: advancements and applications

Space exploration is intrinsically related to spectroscopic techniques; however, with the increasing demand for precision, operation range, and economy of scientific cargo, the viability of single spectroscopic methods has been doubted [202] gives an overview of recently employed spectroscopies, summarising their advantages and drawbacks in Table 3. Overall, as the authors suggest, the need for hyphenated methods in space probing spectroscopy is imminent.

In the context of LIBS space probing, several analytical protocols have been so combined for various kinds of specimens, including those sampled for soil analysis (Sec. 8.2), geochemistry (Sec. 8.1), and, *e.g.*, Ar/K geochronology (*cf* [206–208] and references therein).

Promisingly, a majority of techniques shown Ref. [202] and Table 3 below involve LIBS protocols in their hyphenation. Appreciable efforts have been taken to couple LIBS to the methods of vibrational spectroscopy, either by means of Raman scattering (LIBS–Raman) or, more recently, by those of vibrational infrared spectroscopy and interferometry ((FT)IR–LIBS). The advantage is here taken of the complementation of laser atomic spectroscopy and the analytical information borne by molecular vibrations, as well as of the complementation of IR and Raman techniques. Moreover, such techniques as scanning electron microscopy–electron dispersion spectroscopy (SEM–EDS in Table 3) or, more recently, mass spectrometry, have served as calibration in ground-based LIBS protocols [209].

Since Raman spectroscopy's space applications remarkably surpass those of Fourier transform IR spectroscopy, only the former is discussed below in more detail. In Refs. [210–215], the reader will find additional in-depth description of the latter's techniques and derivatives related to laboratory sampling of space material-like specimens.

Table 3
Comparison of the capabilities of the five systems employed in "this investigation" (reproduced with permission from Ref. [202]).

Laboratory technique	Mineral identification	Elemental composition	Organic detection
Raman spectroscopy	Yes	Inferable (only major elements)	Yes
Microimaging	Yes, for some minerals	No	Yes
FTIR	Yes	No (inferable)	Yes
LIBS	No	Yes	Potentially
LIF	Potentially	No	Yes
SEM–EDS	Yes (imaging)	Yes (qualitative)	Yes
Laboratory technique	**Geological context**	**LIRS instrument mode**	**Rover instrument equivalent**
Raman spectroscopy	Yes (mapping)	Yes (UV Raman)	RLS (ExoMars), SuperCam (Mars 2020), SHERLOC (Mars 2020)
Microimaging	Yes	Yes (target selection)	CLUPI (ExoMars)
FTIR	Yes (mapping)	No (used as a supporting technique)	MicroOmega (ExoMars)
LIBS	Yes (mapping)	Yes	ChemCam (MSL), SuperCam (Mars 2020)
LIF	Yes	Yes	SHERLOC (Mars 2020)
SEM–EDS	No	No	APXS (MSL)

Notes: RLS: Raman laser spectrometer, ChemCam: chemistry and camera, SHERLOC: scanning habitable environments with Raman and luminiscence for organics and chemicals, CLUPI: close-up imager, MicroOmega: micro-observoire pour la mineralogie, l'eua, les glaces et l'activité, APXS: α-particle X-ray spectrometer, MSL: Mars Science Laboratory.

8.1. LIBS–Raman

The LIBS–Raman hyphenation emerged as a natural result of the plasma optical emission and laser scattering phenomena occurring simultaneously during either method's development [216,217]. Various approaches have since been taken to optimize the capture of both events which, in general, may compete with each other – see Fig. 8(A) of [216]. Shown in the diagram is the laser fluence, *i.e.*, its radiation energy per unit surface.

[217,219–221] moreover detail a set-up of two different sources, *e.g.*, a pulsed (typically Nd:YAG LIBS) laser and a continuous-wave (typically 532 nm) Raman laser [217,219]. By careful logic circuiting, Raman scattering is triggered prior to LIP breakdown so as to keep analysing a clean surface. [222], furthermore, carried various performance tests of such a hybrid set-up under conditions relevant to planetary, and namely Martian atmospheres. Very similar rationales were followed by Ref. [223], wherein the experimental constraints of linking LIBS to Raman spectroscopy are translated into a compact spectrometer design.

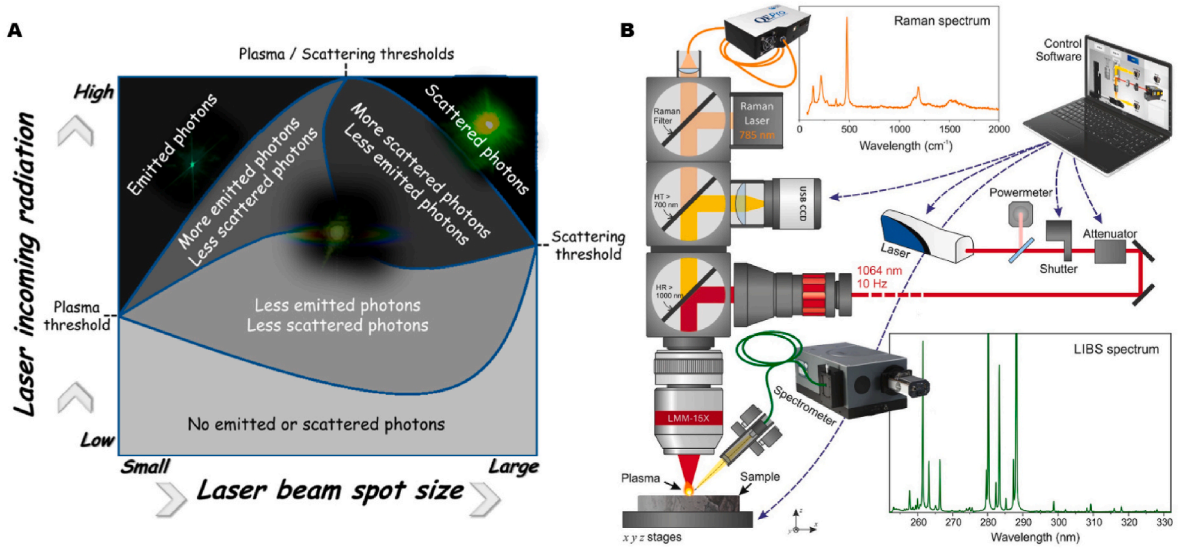

Fig. 8. **(A)** Phenomena diagram for the retrieved photons from laser–matter interaction as a function of the intensity of incident photons and the size of the irradiated area. Reprinted with permission from Ref. [216]. Copyright 2024 American Chemical Society. **(B)** A schematic view of the LIBS–Raman imaging system taken as a typical set-up consisting of 2 laser sources. Reprinted with permission from Ref. [218].

By a series of planetary simulant experiments, insightful implications are drawn for Mars, Venus, and even the Moon [221] and references therein, moreover, overviewed various data processing methods linked to different sources instrumentations.

Hybrid solutions have been imperative to several more layouts, including those assembled for analytical (micro)imaging, *cf.* Table 3 and Fig. 8(B) of [218].

Besides tandem analyses, [217], relied on the post-processing of separate Raman and LIBS records in the form of univariate calibration curves. Raman spectroscopy was then used to quantify a specimen's molecules, or its anionic counterpart, while LIBS served as a proxy for metal cation detection. Remarkably, the LOD of mg kg^{-1} was reached by Raman scattering while order-of-magnitude LODs (10^1–10^3 μg kg^{-1}) were sustained by LIBS. The authors of [224] used a similar LIBS–Raman architecture to analyze mixed geological samples, wherein LIBS's analytical performance was decisively superior to that of Raman scattering.

Nonetheless, pure LIBS analysis was proved incapable of estimating the specimen's anionic contents, namely due to the cumbersome ionization of electronegative species [225,226] therefore uses Raman spectroscopy for mineralogic classification based on (groups of) anions, while LIBS assays later serve for precise quantification. Univariate models are, however, natively suppressed in the case of LIBS–Raman spectromicroscopies. In Ref. [218], a multivariate curve resolution model is supplemented by alternating least squares to mimic applying the Bouguer–Beer–Lambert law on spatially resolved LIBS and Raman mineralogy [227]-based double compression is respectively employed for yielding a data matrix from LIBS imaging data, their Raman counterpart, and a low-level fused data of both former.

Analysing complex minerals thereby is of great importance to space probing [218]; nonetheless remark on a general lack of LIBS–Raman chemometric assays, as well as on difficult experimental optimization of such hybrid set-ups. Encouragingly, however, their bilinear model is, in principle, related to various newly developed FTIR–LIBS data mining protocols described in Ref. [210].

The major drawback of the above strategies is nonetheless the impossibility to ensure the exact same data capture conditions for combined LIBS and Raman sampling (despite the latter's (quasi)-non-destructiveness). Relating back to Fig. 8, another strategy is hence to compromise the energy of single a pulsed laser by irradiating a comparably larger area with collimated beams. As only one source is used, not only sampling conditions but also the set-up portability are enhanced [228] refer to such instrumentation in context of real Mars probing LIBS–Raman missions and offer fundamental chemometrics behind Martian data processing.

Direct contatenation of preprocessed Raman and LIBS spectra (Fig. 9 **C**) are treated with principal component analysis and Euclidean distances of three main clusters are estimated. When compared to those of pure Raman and, respectively LIBS channels (Fig. 9 **A**,–**B**), fused data show distinctively larger cluster distances (intergroup variances) while keeping their sizes (intragroup variances) constant. Any mineral phases present in such real data are thus discriminated with much greater certainty and facility.

[216] rationalise for single-laser set-ups by means of time gating. In particular, various artificial samples relevant to Martian simulants are contemporarily probed by Raman scattering (8 ns of gate width delayed by 38 ns) and LIBS spectroscopy (5 μs of gate width delayed by 50 ns) triggered by a high-fluence pulsed 532 nm laser. Meticulous experimental optimization of the pressure chamber sensing yielded various multimolecular spectral records wherein cationic and anionic signatures are co-sought by a strategic decision tree algorithm. While remarkable success was recorded thereby, a natural follow-up might be to involve correlation spectroscopies [229,230] into the data processing of such neatly optimized experimental records.

LIBS–Raman's double spectroscopy approach also comes with the advantage of cargo reduction, as clearly incentivised by a spatial heterodyne-based LIBS–(line imaging) Raman hyphenation of [231]. Moreover, [202], proved at least comparable applicability of separate set-ups in a simulated Martian mission. A high repetition μLIBS set-up was employed for LIP generation and a 266 nm laser instrumentation was separately carried for both Raman spectroscopy and laser-induced fluorescence. By careful data (post)processing, the authors drew numerous concluding remarks on material analysis in Martian conditions, including, besides the aforementioned mineralogic analytes, organics and CO_2 accompanying their laser plasma decomposition. Promisingly, large importance was ascribed to LIBS mineralogic assays (cf. references above), while an incentive was addressed to verifying such mineralogic correlation by means of (reflectance) FTIR. In real spaceborne conditions, however, mass spectrometry and its LIBS hyphenation are foreseen being handier validation techniques, since, *vide infra*, their sample preparation is considerably easier than in the case of (laboratory) FTIR.

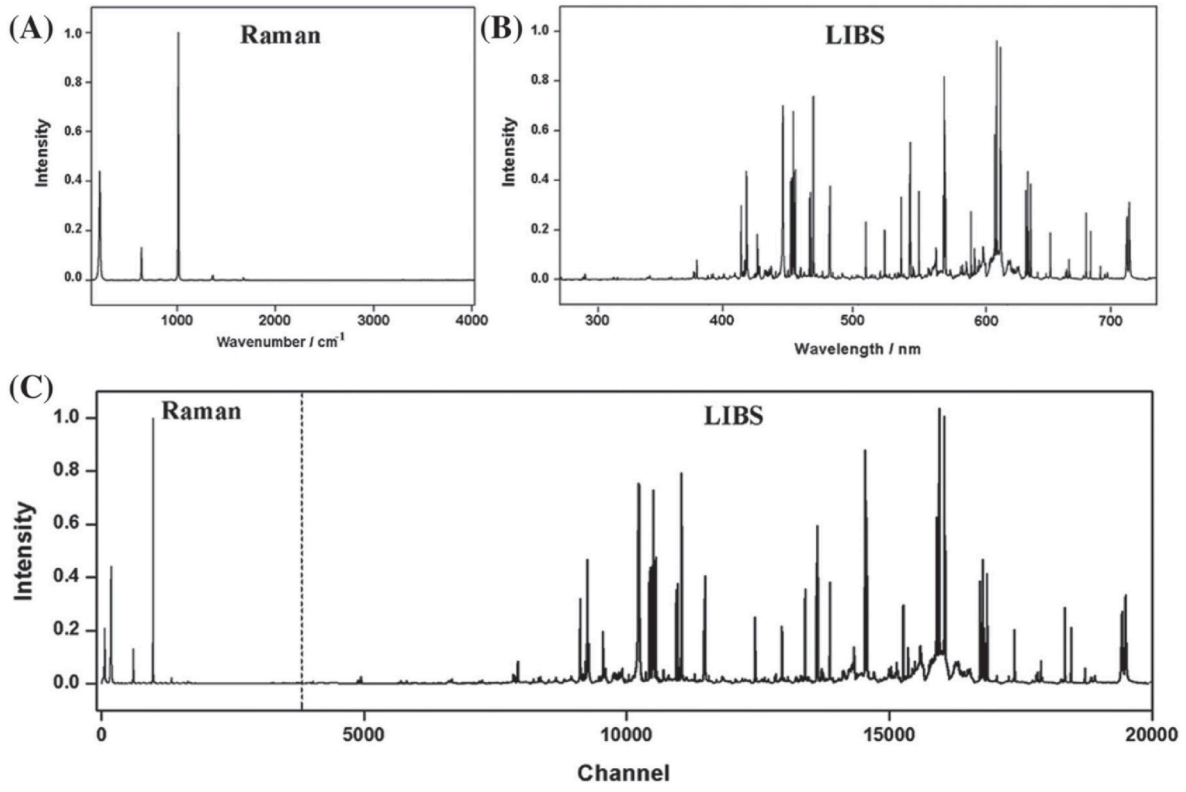

Fig. 9. "(**A**) baseline-corrected Raman spectra, (**B**) LIBS spectra, and (**C**) low-level fused Raman-LIBS spectra collected from the calcium carbonate sample" captured by single laser instrumentation of [228]. Reprinted with permission from Ref. [228].

At the end of this subsection, we present one example of the application of several spectroscopic methods during the geological survey of the Mars surface in the area of the Floor of Jezero Crater [75]. This study was focused on carbonate detection with SuperCam analytical methods: LIBS, infrared reflectance spectroscopy (IRS), and time-resolved Raman (TRR) spectroscopy. Carbonates were identified by directly detecting vibrational modes of CO_3 functional groups (IRS and TRR), major oxides content, and ratios of C and O signal intensities (LIBS). Carbonates are minerals that typically form when primary magmatic minerals undergo alteration. This process can happen under various environmental conditions, which influence the resulting carbonate's quantity and composition. As a result, carbonates reflect the conditions present during their formation, especially the levels of CO_2 and liquid water involved. Studying the history of water and CO_2 on Mars is crucial for understanding the planet's evolution. Since Carbonates were found in low amounts, the authors used a specifically developed methodology to strengthen the identification of carbonate phases and their characterization. Despite this effort, in several targets carbonates were detected by some of the techniques but less confidently or not at all by other techniques. The authors explain this observation by a combination of several factors. One of them is that the analytical footprints of the used techniques are different, varying between, for example, 0.35 mm for LIBS and 4.6 mm for IRS for a target at 4 m. This, together with the targets' heterogeneity can cause significant discrepancies between the techniques. In the study, 220+ targets were analyzed from which approximately 30–40 contained carbonate mineral phases.

8.2. Mass spectrometry–LIBS

Hyphenating mass spectrometry methods to LIBS represents an intuitive step, given that the former has often served as a calibration technique for the latter's results and multispectral assays based thereupon (see references in Ref. [209] for general exemplifications). The development of High-Resolution Mass Spectrometers (HRMS) marks the next critical step in determining the precise composition of unknown extraterrestrial materials. The necessity for high-resolution mass spectrometers for space applications became apparent following the recent Cassini-Huygens missions [232]—the parameters of the Cosmic Dust Analyzer (CDA) ($m/\Delta m = 50$) were not sufficient to resolve complex mixtures of simple hydrocarbons—and the Rosetta mission [233], where the mass spectrometer achieved a resolution of $m/\Delta m = 3000$.

For the forthcoming NASA Europa Clipper mission, a high-resolution mass spectrometer named the Mass SPectrometer for Planetary EXploration (MASPEX) is under development [234]. This instrument is reported to achieve a mass resolution of approximately $m/\Delta m = 7000$ at $m/z = 80$, which is crucial for identifying simple hydrocarbons (CxHy) in various gas mixtures.

However, mass spectrometers with mass resolutions up to 50,000 or beyond are poised to play a central role in acquiring qualitatively novel data types. One example is the commercial orbitrap spectrometer developed by Prof. Makarov [237]. The initial pilot study [238] paved the way for these new types of mass analyzers in space applications. Subsequent research [239,240] utilizing new laboratory prototypes (CosmOrbitrap, OLYMPIA-Orbitrap Analyzer for Multiple Ionization, HANKA-Mass Analyzer for Space Applications) has validated this approach, both for laboratory analogs of space objects and for the development of instruments capable of immediate analysis directly on the spacecraft. Notably, the development of HANKA is currently underway, with a concept for a LILA system that combines LIBS and the HANKA mass spectrometer into a LIBS/orbiMS instrument attached to a robotic arm, as depicted in Fig. 5, Panel C.

LIBS's role in MS–based hydrocarbon analysis is exemplified by Ref. [241] and, more recently [242], who found various promising LIBS tracers of solid organic matter in Mars-like conditions under the guidance of independent (GC– [243])MS protocols [244,245]. Even pure remote LIBS techniques may therefore corroborate the current quests of organics detection on planets [202] if calibrated or validated by a mass spectrometry reference.

This is well exemplified by Refs. [43,246,247] who built an LIBS calibration protocol relevant to *in situ* conditions of Mars Space Laboratory. In Ref. [43], fabricated silicates were taken as Martian–like glass simulants and analyzed by means of electron probe (major constituents, *cf*. Table 3) and, respectively, laser-assisted ICP–MS (minor to trace elements) [246]focused on ceramics sintered of various planetary geochemical analytes and employed numerous (mass) spectroscopy, diffraction and activation analyses to reliably assess their chemical contents. A net LIBS assay was used here to reveal a specimen's heterogeneity [247] then tackled both such results into a univariate *in situ* LIBS calibration protocol to be involved in Martian expeditions.

Opposed to the above univariate calibration are more recent calibration-free approaches exemplified by Ref. [248] who strove for a compact analysis of rare earth ores. 532 nm pulsed laser experiment of differed energies were used respectively for LIBS (100 mJ, miniature spectrometers) and laser assisted time-of-flight MS (5 mJ, in-house built detection), and both techniques probed the relative mass occurrence of La, Ce, and Nd, alongside with possible matrix interferents (Fe and Si). As a key result, the target analytes were evaluated by a simpler single-element Saha–Boltzmann technique and such results were corroborated by both the LA–TOF–MS and an external asset of an EDX probe. A similar procedure is detailed, *e.g.*, by Ref. [249], this time including self-absorption corrections of LIBS data. While this approach entails careful verification of CF–LIBS's physical assumptions, it holds great promise for facile tracing of rare earth metals in matrices without matched standards. Remarkably good correlations between such analytical methods moreover strengthen the claim of [250] where LIBS is untypically proposed as a self-standing internal standards for MS protocols.

Even more pronounced are recent multivariate approaches to dual MS–LIBS analytical imaging, as exemplified by Ref. [235] for data fusion of parallel LIBS (1064 nm Nd:YAG) and LA–ICP–MS (213 nm LSX 213 G2) spectromicroscopies. Not only methodologic but also spatial complementation (*cf*. Fig. 10) was employed in this study, and comprehensive software was developed to study the distribution and migration of mineral analytes in an ore. As detailed further in 8.1, such coupled analytical imaging has vast future implications for probing heterogeneous solids in the universe.

[250] also foreshadowed the usage of tandem hyphenation, which is perhaps more common in the LIBS–Raman method (8.1) [236] nonetheless give a motivation for a coupled laser-assisted MS sensor and arrive at optimizing its set-up as follows in Fig. 10. Therein, plasma generated by pulsed 213 nm Nd:YAG laser ablation of coal is monitored by a Czerny–Turner ICCD spectrograph and, simultaneously, by a commercial ICP–TOF detector. For data curation, the authors relied on PLSR method, drawing upon protocols reviewed for similar specimens in vibrational IR [210]. While PLSR was proven superior to univariate alternatives within each separate method, a physical correlation was moreover found between the mass signal of trace elements and the optical emission of the matrix. Eventually, concatenated ICP–TOF–LIBS data revealed lesser biases in analysing "unknown" (*i.e.*, validation) test samples. Such similar findings are vital to the analysis of complex soils relevant to planetary geochemistry (see also [210] for IR examples).

The authors elaborated on such findings in a more recent study [251] in which tandem LIBS and ICP–TOF–MS fusion is investigated by means of respectively *k*–means PCA [252], partial least squares [210], and support vector machines [253]. As a sound conclusion, concatenated MS–LIBS data again proved superior to those of an individual method, in terms of both sample identification and classification striven for by this study.

Of further importance is a similar tandem set-up of joint LIBS and LA–TOF–MS approach for classifying mineral phases of nephrite jades [254]. Remarkably, both LIBS and MS results were found distinctive for unambiguous classification of a particular jade phase, holding promise for *in situ* mineral analysis.

[255] moreover describe a LIBS–TOF–MS coanalysis of metals and alloys as held under vacuum (10^{-6} Torr) conditions, revealing experimental optimization variables related to (mass) spectral resolution and detection limits, as well as to ion lifetimes in the system. Remarkably, since certain LIBS optima were counteracted by those of the MS protocols, this study pinpoints various experimental trends to be followed by future spaceborne MS–LIBS systems.

As a recent development example, the LIBS/orbiMS instrument LILA is based on heritage from the development of the SLAVIA (Space Laboratory for Advanced Variable Instruments and Applications) mission, focused on the combined exploration of interplanetary matter using the HANKA orbitrap spectrometer and analysis of meteor plasma using the hyperspectral camera Vesna [121]. The concept integrates these two miniaturized instruments mounted on a robotic arm. While LIBS will provide bulk elemental analysis, the orbitrap spectrometer will return data on the content of trace elements, including isotopic composition. A combination of such data will also enable the identification of minerals

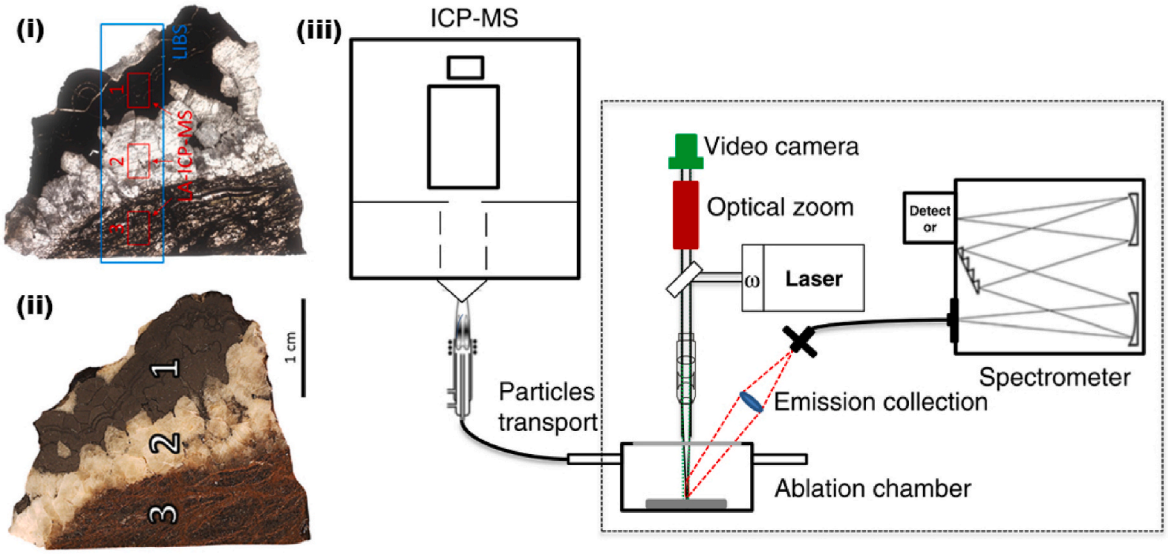

Fig. 10. A cross-section through (**i**) hand specimen and (**ii**) polished thin section of U-mineralisation closely associated with metasomatite and carbonate vein (see Ref. [235] for detailed description) used for elemental distribution maps. Reproduced with permission as a case study of [235]. (**iii**) A schematic system of the tandem LIBS–LA–ICP–TOF–MS [236].

or rocks.

9. Conclusions

Optical Emission Spectroscopy (OES), particularly Laser-Induced Breakdown Spectroscopy (LIBS), has emerged as a valuable tool for space exploration and celestial body prospecting. Despite the challenges posed by different atmospheres, limited calibration possibilities, and instrumental limitations, OES-based methods have been successfully employed in various space missions, providing valuable insights into the composition and characteristics of celestial bodies.

The use of LIBS payloads on Mars rovers, such as NASA's ChemCam and SuperCam, has been instrumental in advancing our understanding of the Martian surface. The recent and forthcoming results from these missions, along with the potential contributions from the Chinese Zhurong rover's MarSCoDe LIBS payload, will continue to expand our knowledge of Mars and pave the way for future missions.

Furthermore, the extreme temperature and atmospheric pressure of Venus present unique challenges for lander missions. However, LIBS has the potential to play a vital role in geochemical investigations on Venus, providing valuable information within the limited timeframe before the instruments succumb to the harsh environment.

Despite setbacks encountered during the Pragyan rover landing, the Moon holds great potential for LIBS-based geological prospecting. However, overcoming the challenges posed by the extreme-high vacuum conditions is crucial for successful LIBS analysis of lunar regolith, and dedicated analytical protocols are required to ensure accurate and reliable results.

As potential mining targets, asteroids require thorough prospecting to assess their composition and resources. LIBS feels promising in this field as well, as indicated by successful chemical analyses of meteorites. LIBS plays a crucial role in providing detailed chemical composition profiles of such systems, aiding in our understanding of planetary evolution and resource potential.

In data processing, transfer learning techniques have shown potential in mitigating the re-calibration burden of LIBS instruments deployed in various atmospheric conditions and experimental settings. In addition, spectral pre-processing and using linear and nonlinear models enhance the accuracy and robustness of LIBS data analysis for space applications. Additionally, hyphenated methods, such as LIBS-Raman, MS-LIBS, and FTIR-LIBS, extend LIBS's capabilities, enabling comprehensive chemical analysis, elemental analysis, and molecular characterisation. These techniques provide valuable insights into celestial bodies' composition, structure, and properties, further enhancing our understanding of the universe.

To summarize, OES, emphasizing LIBS, has revolutionised space exploration and celestial body prospecting. The advancements and applications of LIBS in various space missions have provided valuable data and insights, contributing to our knowledge of Mars, Venus, the Moon, asteroids, and meteorites. As technology advances, further enhancement in data processing, instrument capabilities, and hyphenated methods will propel our understanding of the cosmos and open up new possibilities for future space exploration. in data processing, instrument capabilities, and hyphenated methods will propel our understanding of the universe and open up new possibilities for future space exploration.

CRediT authorship contribution statement

H. Saeidfirozeh: Writing – review & editing, Writing – original draft, Investigation. **P. Kubelík:** Writing – review & editing, Writing – original draft, Investigation. **V. Laitl:** Writing – original draft, Investigation. **A. Křivková:** Writing – original draft, Investigation. **J. Vrábel:** Writing – original draft, Investigation. **K. Rammelkamp:** Writing – review & editing, Writing – original draft, Investigation. **S. Schröder:** Writing – review & editing, Writing – original draft, Funding acquisition, Formal analysis. **I.B. Gornushkin:** Writing – original draft, Investigation. **E. Képeš:** Writing – original draft. **J. Žabka:** Writing – original draft. **M. Ferus:** Writing – review & editing, Writing – original draft, Funding acquisition, Conceptualization. **P. Pořízka:** Writing – review & editing, Writing – original draft, Project administration, Conceptualization. **J. Kaiser:** Supervision, Funding acquisition.

Declaration of competing interest

The authors declare that they have no known competing financial interests or personal relationships that could have appeared to influence the work reported in this paper.

Acknowledgements

All authors would like to acknowledge the financial support of the Czech Science Foundation (GACR) under grant number 23–05186K, and German Research Foundation (DFG). MF, HS would like to acknowledge the financial support of the Technology Agency of the Czech Republic (TAČR, NCK) under the grant under TN02000009/07 FREYA. We also greatly acknowledge the support of the regional collaboration with Valašské Meziříčí observatory provided by a grant of reg. no. R200402401. JV is grateful for the support from project CEITEC VUT-J-23-8332. PP and JK acknowledge the support of Brno University of Technology (FSI–S-23-8389). The authors acknowledge the assistance provided by the Advanced Multiscale Materials for Key Enabling Technologies project, supported by the Ministry of Education, Youth, and Sports of the Czech Republic. Project No. CZ.02.01.01/00/22 008/0004558, Co-funded by the European Union.

Data availability

No data was used for the research described in the article.

References

[1] A.K. Knight, N.L. Scherbarth, D.A. Cremers, M.J. Ferris, Characterization of laser-induced breakdown spectroscopy (libs) for application to space exploration, Appl. Spectrosc. 54 (3) (2000) 331–340.
[2] R.C. Wiens, X. Wan, J. Lasue, S. Maurice, Chapter 20 - laser-induced breakdown spectroscopy in planetary science, in: J.P. Singh, S.N. Thakur (Eds.), Laser-Induced Breakdown Spectroscopy, second ed., Elsevier, Amsterdam, 2020, pp. 441–471, https://doi.org/10.1016/B978-0-12-818829-3.00020-4, second edition edition.
[3] D.A. Cremers, Space Applications of LIBS, Springer Berlin Heidelberg, Berlin, Heidelberg, 2014, pp. 257–291, https://doi.org/10.1007/978-3-642-45085-3_10.
[4] L. Radziemski, D. Cremers, A brief history of laser-induced breakdown spectroscopy: from the concept of atoms to libs 2012, Spectrochim. Acta, Part B 87 (2013) 3–10, https://doi.org/10.1016/j.sab.2013.05.013. Thematic Issue: 7th International Conference on Laser Induced Breakdown Spectroscopy (LIBS 2012), Luxor, Egypt, 29 September-4 October 2012.
[5] R. Sagdeev, G. Managadze, I. Shutyaev, K. SzegÄ, P. Timofeev, Methods of remote surface chemical analysis for asteroid missions, Adv. Space Res. 5 (2) (1985) 111–120, https://doi.org/10.1016/0273-1177(85)90394-1.
[6] J.D. Blacic, D.R. Pettit, D.A. Cremers, N. Roessler, Laser-induced breakdown spectroscopy for remote elemental analysis of planetary surfaces, in: Conference: Laser-Induced Breakdown Spectroscopy for Remote Elemental Analysis of Planetary Surfaces, vol. 12, 1992.
[7] A. Knight, N. Scherbarth, D. Cremers, M. Ferris, Characterization of laser-induced breakdown spectroscopy (libs) for application to space exploration, Appl. Spectrosc. 54 (3) (MAR 2000) 331–340, https://doi.org/10.1366/0003702001949591.
[8] B. Sallé, et al., Comparative study of different methodologies for quantitative rock analysis by laser-induced breakdown spectroscopy in a simulated martian atmosphere, Spectrochim. Acta, Part B 61 (3) (2006) 301–313, https://doi.org/10.1016/j.sab.2006.02.003.
[9] J.P. Grotzinger, et al., Mars science laboratory mission and science investigation, Space Sci. Rev. 170 (1–4) (SEP 2012) 5–56, https://doi.org/10.1007/s11214-012-9892-2.
[10] S. Maurice, et al., The chemcam instrument suite on the mars science laboratory (msl) rover: science objectives and mast unit description, Space Sci. Rev. 170 (2012) 95–166, https://doi.org/10.1007/s11214-012-9912-2.
[11] X. Liu, et al., Development and testing of the marscode libs calibration target in China's tianwen-1 mars mission, Space Sci. Rev. 219 (5) (2023) 43, https://doi.org/10.1007/s11214-023-00987-7.

[12] R.C. Wiens, et al., The chemcam instrument suite on the mars science laboratory (msl) rover: body unit and combined system tests, Space Sci. Rev. 170 (2012) 167–227, https://doi.org/10.1007/s11214-012-9902-4.

[13] S. Maurice, et al., Chemcam activities and discoveries during the nominal mission of the mars science laboratory in gale crater, mars, J. Anal. At. Spectrom. 31 (4) (2016) 863–889, https://doi.org/10.1039/C5JA00417A.

[14] V. Rai, S.N. Thakur, Chapter 4 - physics and dynamics of plasma in laser-induced breakdown spectroscopy, in: J.P. Singh, S.N. Thakur (Eds.), Laser-Induced Breakdown Spectroscopy, second ed., Elsevier, Amsterdam, 2020, pp. 71–106, https://doi.org/10.1016/B978-0-12-818829-3.00004-6, second edition edition.

[15] A. Křivková, et al., Morphology of meteorite surfaces ablated by high-power lasers: review and applications, Appl. Sci. 12 (10) (2022) 4869, https://doi.org/10.3390/app12104869.

[16] A. De Giacomo, M. Dell'Aglio, O. De Pascale, S. Longo, M. Capitelli, Laser induced breakdown spectroscopy on meteorites, Spectrochim. Acta, Part B 62 (12) (2007) 1606–1611, https://doi.org/10.1016/j.sab.2007.10.004.

[17] J. Liu, et al., Evidence of water on the lunar surface from chang'e-5 in-situ spectra and returned samples, Nat. Commun. 13 (1) (2022) 3119, https://doi.org/10.1038/s41467-022-30807-5.

[18] M. Ferus, et al., Main spectral features of meteors studied using a terawatt-class high-power laser, Astron. Astrophys. 630 (2019) A127.

[19] D.A. Cremers, A.K. Knight, *Laser-Induced Breakdown Spectroscopy*, Chapter Atomic Spectroscopy, John Wiley and Sons, Ltd, September 2006, pp. 1–25, https://doi.org/10.1002/9780470027318.a5110t, 1.

[20] A.A. Bol'shakov, X. Mao, J.J. González, R.E. Russo, Laser ablation molecular isotopic spectrometry (lamis): current state of the art, J. Anal. At. Spectrom. 31 (1) (2016) 119–134, https://doi.org/10.1039/C5JA00310E.

[21] D.W. Hahn, N. Omenetto, Laser-induced breakdown spectroscopy (libs), part i: review of basic diagnostics and plasma–particle interactions: still-challenging issues within the analytical plasma community, Appl. Spectrosc. 64 (12) (2010) 335A–366A.

[22] F.J. Fortes, J. Moros, P. Lucena, L.M. Cabalín, J.J. Laserna, Laser-induced breakdown spectroscopy, Anal. Chem. 85 (2) (2013) 640–669, https://doi.org/10.1021/ac303220r.

[23] D.W. Hahn, N. Omenetto, Laser-induced breakdown spectroscopy (libs), part ii: review of instrumental and methodological approaches to material analysis and applications to different fields, Appl. Spectrosc. 66 (4) (2012) 347–419, https://doi.org/10.1366/11-06574.

[24] Z.A. Arp, et al., Feasibility of generating a useful laser-induced breakdown spectroscopy plasma on rocks at high pressure: preliminary study for a venus mission, Spectrochim. Acta, Part B 59 (7) (2004) 987–999, https://doi.org/10.1016/j.sab.2004.05.004.

[25] S.M. Clegg, et al., Planetary geochemical investigations using Raman and laser-induced breakdown spectroscopy, Appl. Spectrosc. 68 (9) (2014) 925–936, https://doi.org/10.1366/13-07386.

[26] P.J. Gasda, et al., Next generation laser-based standoff spectroscopy techniques for mars exploration, Appl. Spectrosc. 69 (2) (2015) 173–192, https://doi.org/10.1366/14-07483.

[27] R. Shu, et al., Laser-induced breakdown spectroscopy based detection of lunar soil simulants for moon exploration, Chin. Opt Lett. 5 (1) (2007) 58–59.

[28] H. Qi, et al., Feasibility study on the application of laser induced breakdown spectroscopy to lunar exploration, J. Infrared Millim. Waves 28 (2009) 93–96.

[29] A.J. Effenberger Jr., J.R. Scott, Effect of atmospheric conditions on libs spectra, Sensors 10 (5) (2010) 4907–4925, https://doi.org/10.3390/s100504907.

[30] J.A. Manrique, et al., Supercam calibration targets: design and development, Space Sci. Rev. 216 (2020) 1–27, https://doi.org/10.1007/s11214-020-00764-w.

[31] A. Laxmiprasad, et al., Laser induced breakdown spectroscope on chandrayaan-2 rover: a miniaturized mid-uv to visible active spectrometer for lunar surface chemistry studies, Curr. Sci. 118 (4) (2020).

[32] R. Gaudiuso, M. Dell'Aglio, O. De Pascale, G.S. Senesi, A. De Giacomo, Laser induced breakdown spectroscopy for elemental analysis in environmental, cultural heritage and space applications: a review of methods and results, Sensors 10 (8) (2010) 7434–7468, https://doi.org/10.3390/s100807434.

[33] J. Novotnỳ, et al., A versatile interaction chamber for laser-based spectroscopic applications, with the emphasis on laser-induced breakdown spectroscopy, Spectrochim. Acta, Part B 101 (2014) 149–154, https://doi.org/10.1016/j.sab.2014.08.004.

[34] J. Lambert, et al., Standoff libs and Raman spectroscopy under venus conditions, in: *41st Annual Lunar And Planetary Science Conference*, Number 1533 in Lunar and Planetary Science Conference, mar 2010, p. 2608.

[35] L. Zimmer, S. Yoshida, Feasibility of laser-induced plasma spectroscopy for measurements of equivalence ratio in high-pressure conditions, Exp. Fluid 52 (2012) 891–904, https://doi.org/10.1007/s00348-011-1151-x.

[36] W. Rapin, et al., μ libs: developing a lightweight elemental micro-mapper for in situ exploration, in: 55th Lunar and Planetary Science Conference, Lunar and Planetary Institute, Houston, 2024. Abstract #2670.

[37] A.K. Knight, N.L. Scherbarth, D.A. Cremers, M.J. Ferris, Characterization of laser-induced breakdown spectroscopy (libs) for application to space exploration, Appl. Spectrosc. 54 (3) (Mar 2000) 331–340.

[38] J.P. Grotzinger, et al., A habitable fluvio-lacustrine environment at yellowknife bay, Gale crater, mars, Science 343 (6169) (jan 2014) 1242777, https://doi.org/10.1126/science.1242777, 1242777.

[39] O. Gasnault, et al., Chemcam: zapping mars for 10 years (and more), in: 54th Lunar and Planetary Science Conference, Lunar and Planetary Institute, Houston, 2023. Abstract #2076.

[40] R.C. Wiens, et al., The supercam instrument suite on the nasa mars 2020 rover: body unit and combined system tests, Space Sci. Rev. 217 (2021) 1–87, https://doi.org/10.1007/s11214-020-00777-5.

[41] W. Xu, et al., The MarSCoDe instrument suite on the mars rover of China's tianwen-1 mission, Space Sci. Rev. 217 (5) (2021) 64, https://doi.org/10.1007/s11214-021-00836-5.

[42] S. Le Mouélic, et al., The ChemCam remote micro-imager at Gale crater: review of the first year of operations on mars, Icarus 249 (mar 2015) 93–107, https://doi.org/10.1016/j.icarus.2014.05.030.

[43] C. Fabre, et al., Onboard calibration igneous targets for the mars science laboratory curiosity rover and the chemistry camera laser induced breakdown spectroscopy instrument, Spectrochim. Acta, Part B 66 (3–4) (mar 2011) 280–289, https://doi.org/10.1016/j.sab.2011.03.012.

[44] S.M. McLennan, et al., Elemental geochemistry of sedimentary rocks at yellowknife bay, Gale crater, mars, Science 343 (6169) (jan 2014) 1244734, https://doi.org/10.1126/science.1244734, 1244734.

[45] N. Mangold, et al., Chemical variations in Yellowknife Bay formation sedimentary rocks analyzed by ChemCam on board the Curiosity rover on Mars, J. Geophys. Res. Planets 120 (3) (mar 2015) 452–482, https://doi.org/10.1002/2014JE004681.

[46] A. Cousin, et al., Geochemistry of the Bagnold dune field as observed by ChemCam and comparison with other aeolian deposits at Gale Crater, J. Geophys. Res. Planets 122 (10) (oct 2017) 2144–2162, https://doi.org/10.1002/2017JE005261.

[47] J. Frydenvang, et al., The chemostratigraphy of the murray formation and role of diagenesis at Vera Rubin ridge in Gale crater, mars, as observed by the ChemCam instrument, J. Geophys. Res. Planets 125 (9) (sep 2020) 1–21, https://doi.org/10.1029/2019JE006320.

[48] C. Bedford, et al., Geochemical variation in the Stimson formation of Gale crater: provenance, mineral sorting, and a comparison with modern Martian dunes, Icarus 341 (December 2019) (may 2020) 113622, https://doi.org/10.1016/j.icarus.2020.113622.

[49] C.C. Bedford, et al., An insight into ancient aeolian processes and post-noachian aqueous alteration in Gale crater, mars, using ChemCam geochemical data from the greenheugh capping unit, J. Geophys. Res. Planets 127 (9) (sep 2022) 1–37, https://doi.org/10.1029/2021JE007100.

[50] E. Dehouck, et al., Bedrock geochemistry and alteration history of the clay-bearing glen torridon region of Gale crater, mars, J. Geophys. Res. Planets 127 (12) (dec 2022), https://doi.org/10.1029/2021JE007103.

[51] V. Sautter, et al., Igneous mineralogy at bradbury rise: the first ChemCam campaign at Gale crater, J. Geophys. Res. Planets 119 (1) (jan 2014) 30–46, https://doi.org/10.1002/2013JE004472.

[52] A. Cousin, et al., Classification of igneous rocks analyzed by ChemCam at Gale crater, Mars, Icarus 288 (may 2017) 265–283, https://doi.org/10.1016/j.icarus.2017.01.014.

[53] P.-Y. Meslin, et al., Soil diversity and hydration as observed by ChemCam at Gale crater, mars, Science 341 (6153) (sep 2013) 1238670, https://doi.org/10.1126/science.1238670, 1238670.

[54] A. Cousin, et al., Compositions of coarse and fine particles in martian soils at gale: a window into the production of soils, Icarus 249 (mar 2015) 22–42, https://doi.org/10.1016/j.icarus.2014.04.052.

[55] J. Lasue, et al., Martian eolian dust probed by ChemCam, Geophys. Res. Lett. 45 (20) (oct 2018), https://doi.org/10.1029/2018GL079210, 10,968–10,977.

[56] M. Nachon, et al., Calcium sulfate veins characterized by ChemCam/Curiosity at Gale crater, Mars, J. Geophys. Res. Planets 119 (9) (2014) 1991–2016, https://doi.org/10.1002/2013JE004588.

[57] M. Nachon, et al., Chemistry of diagenetic features analyzed by ChemCam at pahrump hills, Gale crater, mars, Icarus 281 (jan 2017) 121–136, https://doi.org/10.1016/j.icarus.2016.08.026.

[58] J. Frydenvang, et al., Diagenetic silica enrichment and late-stage groundwater activity in Gale crater, Mars, Geophys. Res. Lett. 44 (10) (may 2017) 4716–4724, https://doi.org/10.1002/2017GL073323.

[59] J. L'Haridon, et al., Chemical variability in mineralized veins observed by ChemCam on the lower slopes of Mount Sharp in Gale crater, Mars, Icarus 311 (2018) 69–86, https://doi.org/10.1016/j.icarus.2018.01.028.

[60] P.J. Gasda, et al., Overview of the morphology and chemistry of diagenetic features in the clay-rich glen torridon unit of Gale crater, mars, J. Geophys. Res. Planets 127 (12) (dec 2022), https://doi.org/10.1029/2021JE007097.

[61] J. L'Haridon, et al., Iron mobility during diagenesis at Vera Rubin ridge, Gale crater, mars, J. Geophys. Res. Planets 125 (11) (nov 2020) 1–24, https://doi.org/10.1029/2019JE006299.

[62] G. David, et al., Analyses of high-iron sedimentary bedrock and diagenetic features observed with ChemCam at Vera Rubin ridge, Gale crater, mars: calibration and characterization, J. Geophys. Res. Planets 125 (10) (oct 2020) 1–26, https://doi.org/10.1029/2019JE006314.

[63] O. Forni, et al., First detection of fluorine on mars: implications for Gale crater's geochemistry, Geophys. Res. Lett. 42 (4) (2015) 1020–1028, https://doi.org/10.1002/2014GL062742.

[64] P.J. Gasda, et al., In situ detection of boron by ChemCam on Mars, Geophys. Res. Lett. 44 (17) (2017) 8739–8748, https://doi.org/10.1002/2017GL074480.

[65] M. Gaft, L. Nagli, N. Eliezer, Y. Groisman, O. Forni, Elemental analysis of halogens using molecular emission by laser-induced breakdown spectroscopy in air, Spectrochim. Acta, Part B 98 (aug 2014) 39–47, https://doi.org/10.1016/j.sab.2014.05.011.

[66] D. Vogt, et al., CaCl and CaF emission in LIBS under simulated martian conditions, Icarus 335 (August 2019) (jan 2020) 113393, https://doi.org/10.1016/j.icarus.2019.113393.
[67] S. Schröder, et al., Hydrogen detection with ChemCam at Gale crater, Icarus 249 (mar 2015) 43–61, https://doi.org/10.1016/j.icarus.2014.08.029.
[68] W. Rapin, et al., Hydration state of calcium sulfates in Gale crater, Mars: identification of bassanite veins, Earth Planet Sci. Lett. 452 (oct 2016) 197–205, https://doi.org/10.1016/j.epsl.2016.07.045.
[69] W. Rapin, et al., Roughness effects on the hydrogen signal in laser-induced breakdown spectroscopy, Spectrochim. Acta, Part B 137 (nov 2017) 13–22, https://doi.org/10.1016/j.sab.2017.09.003.
[70] S. Maurice, et al., The supercam instrument suite on the mars 2020 rover: science objectives and mast-unit description, Space Sci. Rev. 217 (2021) 1–108, https://doi.org/10.1007/s11214-021-00807-w.
[71] J.A. Manrique, et al., SuperCam calibration targets: design and development, Space Sci. Rev. 216 (8) (dec 2020) 138, https://doi.org/10.1007/s11214-020-00764-w.
[72] S. Maurice, et al., In situ recording of Mars soundscape, Nature 605 (7911) (may 2022) 653–658, https://doi.org/10.1038/s41586-022-04679-0.
[73] R.C. Wiens, et al., Compositionally and density stratified igneous terrain in Jezero crater, Mars, Sci. Adv. 8 (34) (aug 2022), https://doi.org/10.1126/sciadv.abo3399.
[74] A. Udry, et al., A mars 2020 perseverance SuperCam perspective on the igneous nature of the máaz formation at Jezero Crater and link with séítah, mars, J. Geophys. Res. Planets 128 (7) (jul 2023) 1–28, https://doi.org/10.1029/2022JE007440.
[75] E. Clavé, et al., Carbonate detection with SuperCam in igneous rocks on the floor of Jezero Crater, mars, J. Geophys. Res. Planets 128 (6) (jun 2023) 1–33, https://doi.org/10.1029/2022JE007463.
[76] O. Beyssac, et al., Petrological traverse of the olivine cumulate séítah formation at Jezero Crater, mars: a perspective from SuperCam onboard perseverance, J. Geophys. Res. Planets 128 (7) (jul 2023), https://doi.org/10.1029/2022JE007638.
[77] X. Liu, et al., Development and testing of the MarSCoDe LIBS calibration target in China's tianwen-1 mars mission, Space Sci. Rev. 219 (5) (aug 2023) 43, https://doi.org/10.1007/s11214-023-00987-7.
[78] S. Liu, et al., A novel adaptive spectral drift correction method for re-calibrating the marscode-libs data in China's tianwen-1 mars mission, J-STARS (2023), https://doi.org/10.1109/JSTARS.2023.3281852.
[79] Y.-Y.S. Zhao, et al., In situ analysis of surface composition and meteorology at the Zhurong landing site on Mars, Natl. Sci. Rev. 10 (6) (may 2023), https://doi.org/10.1093/nsr/nwad056.
[80] Y. Liu, et al., Geological exploration of southern utopia planitia by tianwen-1 zhurong rover, in: 54th Lunar and Planetary Science Conference, Lunar and Planetary Institute, 2023. Abstract #2129, Houston.
[81] A. Ellery, Sustainable in-situ resource utilization on the moon, Planet. Space Sci. 184 (2020) 104870, https://doi.org/10.1016/j.pss.2020.104870.
[82] H. Sato, et al., Lunar mare tio2 abundances estimated from uv/vis reflectance, Icarus 296 (2017) 216–238, https://doi.org/10.1016/j.icarus.2017.06.013.
[83] W. Xia, et al., New maps of lunar surface chemistry, Icarus 321 (2019) 200–215, https://doi.org/10.1016/j.icarus.2018.10.031.
[84] A. Colaprete, et al., Detection of water in the lcross ejecta plume, science 330 (6003) (2010) 463–468, https://doi.org/10.1126/science.1186986.
[85] S. Li, et al., Direct evidence of surface exposed water ice in the lunar polar regions, Proc. Natl. Acad. Sci. USA 115 (36) (2018) 8907–8912, https://doi.org/10.1073/pnas.1802345115.
[86] M.J. Losekamm, et al., Assessing the distribution of water ice and other volatiles at the lunar south pole with luvmi-x: a mission concept, Planet. Sci. J. 3 (10) (2022) 229, https://doi.org/10.3847/PSJ/ac8cfd.
[87] A.S. Laxmiprasad, et al., Laser induced breakdown spectroscope on chandrayaan-2 rover:a miniaturized mid-uv to visible active spectrometer for lunar surface chemistry studies, Curr. Sci. 118 (4) (February 2020) 573, https://doi.org/10.18520/cs/v118/i4/573-581.
[88] A. Laxmiprasad, et al., An in situ laser induced breakdown spectroscope (libs) for chandrayaan-2 rover: ablation kinetics and emissivity estimations, Adv. Space Res. 52 (2) (2013) 332–341, https://doi.org/10.1016/j.asr.2013.03.021.
[89] D.S. Vogt, et al., Voila on the luvmi-x rover: laser-induced breakdown spectroscopy for the detection of volatiles at the lunar south pole, Sensors 22 (23) (December 2022) 9518, https://doi.org/10.3390/s22239518.
[90] K. Rammelkamp, S. Schröder, B.A. Lomax, E. Clavé, H.-W. Hübers, Libs for prospecting and Raman spectroscopy for monitoring: two feasibility studies for supporting in-situ resource utilization, Front. Space Technol 5 (2024) 1336548, https://doi.org/10.3389/frspt.2024.1336548.
[91] S. Schröder, et al., A laser-induced breakdown spectroscopy (libs) instrument for in-situ exploration with the dlr lightweight rover unit (lru), Appl. Sci. 14 (6) (2024) 2467, https://doi.org/10.3390/app14062467.
[92] B. Sallé, D.A. Cremers, S. Maurice, R.C. Wiens, Laser-induced breakdown spectroscopy for space exploration applications: influence of the ambient pressure on the calibration curves prepared from soil and clay samples, Spectrochim. Acta, Part B 60 (4) (2005) 479–490, https://doi.org/10.1016/j.sab.2005.02.009.
[93] J. Lasue, et al., Remote laser-induced breakdown spectroscopy (libs) for lunar exploration, J. Geophys. Res. Planets 117 (E1) (2012), https://doi.org/10.1029/2011JE003898.
[94] K. Yumoto, Y. Cho, S. Kameda, S. Kasahara, S. Sugita, In-situ measurement of hydrogen on airless planetary bodies using laser-induced breakdown spectroscopy, Spectrochim. Acta, Part B 205 (2023) 106696, https://doi.org/10.1016/j.sab.2023.106696.
[95] S. Kubitza, et al., Detecting sulfur on the moon: the potential of vacuum ultraviolet laser-induced breakdown spectroscopy, Spectrochim. Acta, Part B 174 (2020) 105990, https://doi.org/10.1016/j.sab.2020.105990.
[96] J.K. Antony, G.S. Jatana, N.J. Vasa, V.L.N. Sridhar Raja, A.S. Laxmiprasad, Modeling of laser induced breakdown spectroscopy for very low-pressure conditions, Appl. Phys. A 101 (1) (Oct 2010) 161–165, https://doi.org/10.1007/s00339-010-5782-1.
[97] A. Maturilli, J. Helbert, S. Ferrari, B. Davidsson, M. D'Amore, Characterization of asteroid analogues by means of emission and reflectance spectroscopy in the 1-to 100-μm spectral range, Earth Planets Space 68 (2016) 1–11, https://doi.org/10.1186/s40623-016-0489-y.
[98] L.R. Nittler, et al., Bulk element compositions of meteorites: a guide for interpreting remote-sensing geochemical measurements of planets and asteroids, Antarct. Meteor. Res. 17 (January 2004) 231.
[99] E. Jarosewich, Chemical analyses of meteorites: a compilation of stony and iron meteorite analyses, Meteoritics 25 (4) (1990) 323–337, https://doi.org/10.1111/j.1945-5100.1990.tb00717.x.
[100] D. Brownlee, The stardust mission: analyzing samples from the edge of the solar system, Annu. Rev. Earth Planet Sci. 42 (2014) 179–205, https://doi.org/10.1146/annurev-earth-050212-124203.
[101] F. Namouni, M.H.M. Morais, An interstellar origin for high-inclination centaurs, Mon. Not. Roy. Astron. Soc. 494 (2) (2020) 2191–2199, https://doi.org/10.1093/mnras/staa712.
[102] A. Cellino, Asteroids, in: D. Alderton, S.A. Elias (Eds.), Encyclopedia of Geology, second ed., Academic Press, Oxford, 2021, pp. 141–149, https://doi.org/10.1016/B978-0-12-409548-9.11842-1, second edition edition.
[103] M. Elvis, How many ore-bearing asteroids? Planet. Space Sci. 91 (2014) 20–26, https://doi.org/10.1016/j.pss.2013.11.008.
[104] M. Ferus, J. Žabka, N. Schmidt, A. Heays, Asteroid prospecting and space mining, in: Governance of Emerging Space Challenges: the Benefits of a Responsible Cosmopolitan State Policy, Springer, 2022, pp. 217–232, https://doi.org/10.1007/978-3-030-86555-9_12.
[105] S. Pavlov, S. Schröder, I. Rauschenbach, E. Jessberger, H.-W. Hübers, Low-energy laser induced breakdown spectroscopy for in-situ space missions to solar system bodies without atmospheres, Planet. Space Sci. 71 (1) (2012) 57–63, https://doi.org/10.1016/j.pss.2012.07.001.
[106] M. Elvis, Prospecting asteroid resources, Aster: Prospective energy and material resources (2013) 81–129, https://doi.org/10.1007/978-3-642-39244-3_4.
[107] S. Ramasamy, V. Venkatasubrmanian, S. Anbazhagan, Reflectance spectra of minerals and their discrimination using thematic mapper, irs and spot multi-spectral data, Int. J. Rem. Sens. 14 (16) (1993) 2935–2970, https://doi.org/10.1080/01431169308904412.
[108] V. Reddy, T.L. Dunn, C.A. Thomas, N.A. Moskovitz, T.H. Burbine, Mineralogy and surface composition of asteroids, Aster IV (2867) (2015) 43–63.
[109] J.S. Kargel, Metalliferous asteroids as potential sources of precious metals, J. Geophys. Res. Planets 99 (E10) (1994) 21129–21141, https://doi.org/10.1029/94JE02141.
[110] S.J. Ostro, et al., Radar observations of asteroid 216 kleopatra, Science 288 (5467) (2000) 836–839, https://doi.org/10.1126/science.288.5467.836.
[111] P. D'Arrigo, S. Santandrea, The apies mission to explore the asteroid belt, Adv. Space Res. 38 (9) (2006) 2060–2067, https://doi.org/10.1016/j.asr.2006.09.017.
[112] C.R. Chapman, The galileo encounters with gaspra and ida, in: Symposium-International Astronomical Union, vol. 160, Cambridge University Press, 1994, pp. 357–365.
[113] J. Veverka, et al., The landing of the near-shoemaker spacecraft on asteroid 433 eros, Nature 413 (6854) (2001) 390–393, https://doi.org/10.1038/35096507.
[114] M. Ebihara, et al., Chemical and mineralogical compositions of two grains recovered from asteroid itokawa, Meteorit. Planet. Sci. 50 (2) (2015) 243–254, https://doi.org/10.1111/maps.12418.
[115] B. Allen, et al., The regolith x-ray imaging spectrometer (rexis) for osiris-rex: identifying regional elemental enrichment on asteroids, Optical Modeling and Performance Predictions VI 8840 (2013) 142–158. SPIE.
[116] K. Kitazato, et al., The surface composition of asteroid 162173 ryugu from hayabusa2 near-infrared spectroscopy, Science 364 (6437) (2019) 272–275, https://doi.org/10.1126/science.aav743.
[117] G.B. Hughes, et al., DE-STAR: phased-array laser technology for planetary defense and other scientific purposes, in: E.W. Taylor, D.A. Cardimona (Eds.), *Nanophotonics And Macrophotonics For Space Environments VII*, Volume 8876 of *Society Of Photo-Optical Instrumentation Engineers (SPIE) Conference Series*, sep 2013, p. 88760J.
[118] A. Křivková, et al., Application of a dielectric breakdown induced by high-power lasers for a laboratory simulation of meteor plasma, Exp. Astron. 51 (2) (April 2021) 425–451, https://doi.org/10.1007/s10686-020-09688-3.
[119] M. Ferus, et al., Elemental composition, mineralogy and orbital parameters of the porangaba meteorite, Icarus 341 (2020) 113670, https://doi.org/10.1016/j.icarus.2020.113670.
[120] P. Kubelík, et al., Probing plasma physics and elemental composition of a leonid meteor by fitting complex plasma radiation model parameters, Mon. Not. Roy. Astron. Soc. 514 (4) (aug 2022) 5266–5275, https://doi.org/10.1093/mnras/stac1600.
[121] M. Ferus, et al., Simulating asteroid impacts and meteor events by high-power lasers: from the laboratory to spaceborne missions, Front. astron. space sci. 10 (2023) 1186172, https://doi.org/10.3389/fspas.2023.1186172.

[122] D. Ozdín, et al., Mineralogy, petrography, geochemistry, and classification of the košice meteorite, Meteorit. Planet. Sci. 50 (5) (2015) 864–879, https://doi.org/10.1111/maps.12405.
[123] N. S. Todd. Lunar Meteorite Compendium — curator.jsc.nasa.gov. https://curator.jsc.nasa.gov/antmet/lmc/index.cfm. [Accessed 11-June-2024].
[124] N. S. Todd. Martian Meteorite Compendium — curator.jsc.nasa.gov. https://curator.jsc.nasa.gov/antmet/mmc/introduction.cfm. [Accessed 11-June-2024].
[125] M. Granvik, P. Brown, Identification of meteorite source regions in the Solar System, Icarus 311 (September 2018) 271–287, https://doi.org/10.1016/j.icarus.2018.04.012.
[126] M. Baudelet, B. Smith, The first years of laser-induced breakdown spectroscopy, J. Anal. At. Spectrom. 28 (2013) 624, https://doi.org/10.1039/c3ja50027f, 05.
[127] M. Dell'Aglio, et al., Laser Induced Breakdown Spectroscopy applications to meteorites: chemical analysis and composition profiles, Geochem. Cosmochim. Acta 74 (24) (dec 2010) 7329–7339, https://doi.org/10.1016/j.gca.2010.09.018.
[128] J.R. Thompson, et al., Remote laser-induced breakdown spectroscopy analyses of Dar al Gani 476 and Zagami Martian meteorites, J. Geophys. Res. Planets 111 (E5) (May 2006) E05006, https://doi.org/10.1029/2005JE002578.
[129] G.S. Senesi, Laser-Induced Breakdown Spectroscopy (LIBS) applied to terrestrial and extraterrestrial analogue geomaterials with emphasis to minerals and rocks, Earth Sci. Rev. 139 (December 2014) 231–267, https://doi.org/10.1016/j.earscirev.2014.09.008.
[130] M. Dell'Aglio, A. De Giacomo, R. Gaudiuso, O. De Pascale, S. Longo, Laser Induced Breakdown Spectroscopy of meteorites as a probe of the early solar system, Spectrochim. Acta, Part B 101 (November 2014) 68–75, https://doi.org/10.1016/j.sab.2014.07.011.
[131] M. Horňáčková, et al., Calibration-free laser induced breakdown spectroscopy as an alternative method for found meteorite fragments analysis, Eur. Phys. J. Appl. Phys. 66 (1) (April 2014) 10702, https://doi.org/10.1051/epjap/2014130465.
[132] M. Dell'Aglio, M. López-Claros, J.J. Laserna, S. Longo, A. De Giacomo, Stand-off laser induced breakdown spectroscopy on meteorites: calibration-free approach, Spectrochim. Acta, Part B 147 (September 2018) 87–92, https://doi.org/10.1016/j.sab.2018.05.024.
[133] A. Hertzberg, On the Possibility of Simulating Meteoroid Impact by the Use of Lasers Topical Report, NASA, 1964.
[134] B. Hapke, W. Cassidy, E. Wells, Effects of vapor-phase deposition processes on the optical, chemical, and magnetic properties OE the lunar regolith, Moon 13 (1–3) (July 1975) 339–353, https://doi.org/10.1007/BF00567525.
[135] A.N. Pirri, Theory for laser simulation of hypervelocity impact, Phys. Fluids 20 (2) (February 1977) 221–228, https://doi.org/10.1063/1.861859.
[136] A. Křivková, et al., Application of a dielectric breakdown induced by high-power lasers for a laboratory simulation of meteor plasma, Exp. Astron. 51 (2021) 425–451, https://doi.org/10.1007/s10686-020-09688-3.
[137] P. Lubin, et al., Toward directed energy planetary defense, Opt. Eng. 53 (2) (2014) 025103, https://doi.org/10.1117/1.OE.53.2.025103, 025103.
[138] G.B. Hughes, et al., Remote laser evaporative molecular absorption spectroscopy, Planetary defense and space environment applications 9981 (2016) 175–186. SPIE.
[139] R.B. Anderson, et al., Post-landing major element quantification using supercam laser induced breakdown spectroscopy, Spectrochim. Acta, Part B 188 (2022) 106347, https://doi.org/10.1016/j.sab.2021.106347.
[140] G. David, et al., Laser-induced breakdown spectroscopy (libs) characterization of granular soils: implications for chemcam analyses at gale crater, mars, Icarus 365 (2021) 114481, https://doi.org/10.1016/j.icarus.2021.114481.
[141] S.M. Clegg, et al., Recalibration of the mars science laboratory chemcam instrument with an expanded geochemical database, Spectrochim. Acta, Part B 129 (2017) 64–85, https://doi.org/10.1016/j.sab.2016.12.003.
[142] J. Castorena, D. Oyen, A. Ollila, C. Legett, N. Lanza, Deep spectral cnn for laser induced breakdown spectroscopy, Spectrochim. Acta, Part B 178 (2021) 106125, https://doi.org/10.1016/j.sab.2021.106125.
[143] C. Liu, et al., A martian analogues library (mal) applicable for tianwen-1 marscode-libs data interpretation, Rem. Sens. 14 (12) (2022) 2937, https://doi.org/10.3390/rs14122937.
[144] C. Sun, et al., From machine learning to transfer learning in laser-induced breakdown spectroscopy analysis of rocks for mars exploration, Sci. Rep. 11 (1) (2021) 21379, https://doi.org/10.1038/s41598-021-00647-2.
[145] L.-N. Li, X.-F. Liu, W.-M. Xu, J.-Y. Wang, R. Shu, A laser-induced breakdown spectroscopy multi-component quantitative analytical method based on a deep convolutional neural network, Spectrochim. Acta, Part B 169 (2020) 105850, https://doi.org/10.1016/j.sab.2020.105850.
[146] F.T. Liu, K.M. Ting, Z.-H. Zhou, Isolation-based anomaly detection, ACM Trans. Knowl. Discov. Data 6 (1) (mar 2012), https://doi.org/10.1145/2133360.2133363.
[147] P.J. Gasda, et al., Quantification of manganese for chemcam mars and laboratory spectra using a multivariate model, Spectrochim. Acta, Part B 181 (2021) 106223, https://doi.org/10.1016/j.sab.2021.106223.
[148] M. Konstantinidis, et al., Elemental estimation of terrestrial analogues from the canmars rover field campaign using lirs: implications for detecting silica-rich deposits on mars, Icarus 358 (2021) 114113, https://doi.org/10.1016/j.icarus.2020.114113.
[149] C.R. Ytsma, M.D. Dyar, Effects of univariate and multivariate regression on the accuracy of hydrogen quantification with laser-induced breakdown spectroscopy, Spectrochim. Acta, Part B 139 (2018) 27–37, https://doi.org/10.1016/j.sab.2017.11.010.
[150] E. Képeš, P. Pořízka, J. Kaiser, On the application of bootstrapping to laser-induced breakdown spectroscopy data, J. Anal. At. Spectrom. 34 (12) (2019) 2411–2419, https://doi.org/10.1039/C9JA00304E.
[151] S. Shabbir, et al., Machine learning and transfer learning for correction of the chemical and physical matrix effects in the determination of alkali and alkaline earth metals with libs in rocks, Spectrochim. Acta, Part B 194 (2022) 106478, https://doi.org/10.1016/j.sab.2022.106478.
[152] K.H. Lepore, C.R. Ytsma, M.D. Dyar, Quantitative prediction accuracies derived from laser-induced breakdown spectra using optimized multivariate submodels, Spectrochim. Acta, Part B 191 (2022) 106408, https://doi.org/10.1016/j.sab.2022.106408.
[153] Y. Yu, M. Yao, When convolutional neural networks meet laser-induced breakdown spectroscopy: end-to-end quantitative analysis modeling of chemcam spectral data for major elements based on ensemble convolutional neural networks, Rem. Sens. 15 (13) (2023) 3422, https://doi.org/10.3390/rs15133422.
[154] J. Castorena, D. Oyen Spectroscopynet, Learning to pre-process spectroscopy signals without clean data, in: 2022 56th Asilomar Conference on Signals, Systems, and Computers, 2022, pp. 960–964.
[155] H. Bai, et al., Application of elastic net in quantitative analysis of major elements using martian laser-induced breakdown spectroscopy datasets, Spectrochim. Acta, Part B 199 (2023) 106587, https://doi.org/10.1016/j.sab.2022.106587.
[156] S.M. Clegg, E. Sklute, M.D. Dyar, J.E. Barefield, R.C. Wiens, Multivariate analysis of remote laser-induced breakdown spectroscopy spectra using partial least squares, principal component analysis, and related techniques, Spectrochim. Acta, Part B 64 (1) (2009) 79–88, https://doi.org/10.1016/j.sab.2008.10.045.
[157] M.D. Dyar, et al., Comparison of univariate and multivariate models for prediction of major and minor elements from laser-induced breakdown spectra with and without masking, Spectrochim. Acta, Part B 123 (2016) 93–104, https://doi.org/10.1016/j.sab.2016.07.010.
[158] X. Liu, et al., Comparison on quantitative analysis of olivine using marscode laser-induced breakdown spectroscopy in a simulated martian atmosphere, Rem. Sens. 14 (21) (2022) 5612, https://doi.org/10.3390/rs14215612.
[159] F. Yang, et al., Convolutional neural network chemometrics for rock identification based on laser-induced breakdown spectroscopy data in tianwen-1 pre-flight experiments, Rem. Sens. 14 (21) (2022) 5343, https://doi.org/10.3390/rs14215343.
[160] G. Jin, et al., A new spectral transformation approach and quantitative analysis for marscode laser-induced breakdown spectroscopy (libs) data, Rem. Sens. 14 (16) (2022) 3960, https://doi.org/10.3390/rs14163960.
[161] S. Schröder, K. Rammelkamp, D. Vogt, O. Gasnault, H.-W. Hübers, Contribution of a martian atmosphere to laser-induced breakdown spectroscopy (libs) data and testing its emission characteristics for normalization applications, Icarus 325 (2019) 1–15, https://doi.org/10.1016/j.icarus.2019.02.017.
[162] Y. Rao, et al., Transfer learning based on dynamic time warping algorithms to improve qualitative analysis and quantitative prediction of rocks over multiple libs instruments, J. Anal. At. Spectrom. 38 (3) (2023) 693–703, https://doi.org/10.1039/D2JA00370H.
[163] T. Zhou, L. Zhang, Z. Ling, Z. Wu, Z. Shen, Calibration transfer for chemcam spectral data from different laser-induced breakdown spectrometers via a deep extreme learning machine, J. Appl. Spectrosc. 89 (5) (2022) 1002–1013, https://doi.org/10.1007/s10812-022-01459-6.
[164] Z. Chen, et al., Probabilistic multivariable calibration for major elements analysis of marscode martian laser-induced breakdown spectroscopy instrument on zhurong rover, Spectrochim. Acta, Part B 197 (2022) 106529, https://doi.org/10.1016/j.sab.2022.106529.
[165] F. Yang, et al., Laser-induced breakdown spectroscopy combined with a convolutional neural network: a promising methodology for geochemical sample identification in tianwen-1 mars mission, Spectrochim. Acta, Part B 192 (2022) 106417, https://doi.org/10.1016/j.sab.2022.106417.
[166] C.R. Ytsma, M.D. Dyar, Calculations of and effects on quantitative limits for multivariate analyses of geological materials with laser-induced breakdown spectroscopy, Spectrochim. Acta, Part B 191 (2022) 106395, https://doi.org/10.1016/j.sab.2022.106395.
[167] K. Rammelkamp, et al., Clustering supported classification of chemcam data from gale crater, mars, Earth Space Sci. 8 (12) (2021) e2021EA001903, https://doi.org/10.1029/2021EA001903.
[168] L. Han, F. Liu, L. Zhang, An improved sub-model plsr quantitative analysis method based on svm classifier for chemcam laser-induced breakdown spectroscopy, Symmetry 13 (2) (2021) 319, https://doi.org/10.3390/sym13020319.
[169] M.D. Dyar, C.R. Ytsma, Effect of data set size on geochemical quantification accuracy with laser-induced breakdown spectroscopy, Spectrochim. Acta, Part B 177 (2021) 106073, https://doi.org/10.1016/j.sab.2021.106073.
[170] L. Zhang, Z. Wu, Z. Ling, Particle swarm optimization (pso) for improving the accuracy of chemcam libs sub-model quantitative method, Earth Sci. Inform. 13 (2020) 1485–1497, https://doi.org/10.1007/s12145-020-00497-y.
[171] C. Xueqiang, et al., Quantitative analysis modeling for the chemcam spectral data based on laser-induced breakdown spectroscopy using convolutional neural network, Plasma Sci. Technol. 22 (11) (2020) 115502, https://doi.org/10.1088/2058-6272/aba5f6.
[172] C.R. Ytsma, et al., Accuracies and detection limits of major, minor, and trace element quantification in rocks by portable laser-induced breakdown spectroscopy, Spectrochim. Acta, Part B 171 (2020) 105946, https://doi.org/10.1016/j.sab.2020.105946.

[173] K. Rammelkamp, et al., Low-level libs and Raman data fusion in the context of in situ mars exploration, J. Raman Spectrosc. 51 (9) (2020) 1682–1701, https://doi.org/10.1002/jrs.5615.
[174] C.R. Ytsma, M.D. Dyar, Accuracies of lithium, boron, carbon, and sulfur quantification in geological samples with laser-induced breakdown spectroscopy in mars, earth, and vacuum conditions, Spectrochim. Acta, Part B 162 (2019) 105715, https://doi.org/10.1016/j.sab.2019.105715.
[175] P. Pořízka, et al., On the utilization of principal component analysis in laser-induced breakdown spectroscopy data analysis, a review, Spectrochim. Acta, Part B 148 (2018) 65–82, https://doi.org/10.1016/j.sab.2018.05.030.
[176] J. Vrábel, E. Képeš, P. Pořízka, J. Kaiser, Artificial neural networks for classification, Chemom. Numer. Methods LIBS (2022) 213–240, https://doi.org/10.1002/9781119759614.ch9.
[177] E. Képeš, et al., Machine learning in the context of laser-induced breakdown spectroscopy, Laser Induced Breakdown Spectroscopy (LIBS) Concepts, Instrumentation, Data Analysis and Applications 1 (2023) 305–330, https://doi.org/10.1002/9781119758396.ch15.
[178] E. Képeš, et al., Interpreting neural networks trained to predict plasma temperature from optical emission spectra, J. Anal. At. Spectrom. 39 (4) (2024) 1160–1174.
[179] H. Saeidfirozeh, et al., Ann-libs analysis of mixture plasmas: detection of xenon, J. Anal. At. Spectrom. 37 (9) (2022) 1815–1823.
[180] E. Képeš, J. Vrábel, P. Pořízka, J. Kaiser, Improving laser-induced breakdown spectroscopy regression models via transfer learning, J. Anal. At. Spectrom. 37 (9) (2022) 1883–1893, https://doi.org/10.1039/D2JA00180B.
[181] J. Vrábel, et al., Spectral library transfer between distinct laser-induced breakdown spectroscopy systems trained on simultaneous measurements, J. Anal. At. Spectrom. 38 (4) (2023) 841–853, https://doi.org/10.1039/D2JA00406B.
[182] I.B. Gornushkin, V. Veiko, Y.Y. Karlagina, A. Samokhvalov, D. Polyakov, Equilibrium model of titanium laser induced plasma in air with reverse deposition of titanium oxides, Spectrochim. Acta, Part B 193 (2022) 106449, https://doi.org/10.1016/j.sab.2022.106449.
[183] M. Capitelli, A. Casavola, G. Colonna, A. De Giacomo, Laser-induced plasma expansion: theoretical and experimental aspects, Spectrochim. Acta, Part B 59 (3) (2004) 271–289, https://doi.org/10.1016/j.sab.2003.12.017.
[184] J. Van Dijk, G. Kroesen, A. Bogaerts, Plasma modelling and numerical simulation, J. Phys. D Appl. Phys. 42 (19) (2009) 190301, https://doi.org/10.1088/0022-3727/42/19/190301.
[185] I.B. Gornushkin, U. Panne, Radiative models of laser-induced plasma and pump-probe diagnostics relevant to laser-induced breakdown spectroscopy, Spectrochim. Acta, Part B 65 (5) (2010) 345–359, https://doi.org/10.1016/j.sab.2010.03.021.
[186] A. Bogaerts, Z. Chen, R. Gijbels, A. Vertes, Laser ablation for analytical sampling: what can we learn from modeling? Spectrochim. Acta, Part B 58 (2003) 1867–1893, https://doi.org/10.1016/j.sab.2003.08.004.
[187] S. Anisimov, D. Bäuerle, B. Luk'Yanchuk, Gas dynamics and film profiles in pulsed-laser deposition of materials, Phys. Rev. B 48 (16) (1993) 12076, https://doi.org/10.1103/PhysRevB.48.12076.
[188] J. Kools, T. Baller, S. De Zwart, J. Dieleman, Gas flow dynamics in laser ablation deposition, J. Appl. Phys. 71 (9) (1992) 4547–4556, https://doi.org/10.1063/1.350772.
[189] I. Gornushkin, A.Y. Kazakov, N. Omenetto, B. Smith, J. Winefordner, Radiation dynamics of post-breakdown laser induced plasma, Spectrochim. Acta, Part B 59 (4) (2004) 401–418, https://doi.org/10.1016/j.sab.2003.12.023.
[190] I. Gornushkin, S. Shabanov, N. Omenetto, J. Winefordner, Nonisothermal asymmetric expansion of laser induced plasmas into vacuum, J. Appl. Phys. 100 (7) (2006), https://doi.org/10.1063/1.2345460.
[191] R. Kelly, On the dual role of the knudsen layer and unsteady, adiabatic expansion in pulse sputtering phenomena, J. Chem. Phys. 92 (8) (1990) 5047–5056, https://doi.org/10.1063/1.458540.
[192] N. Arnold, J. Gruber, J. Heitz, Spherical expansion of the vapor plume into ambient gas: an analytical model, Appl. Phys. A 69 (1999) S87–S93, https://doi.org/10.1007/s003399900183.
[193] S.-B. Wen, X. Mao, R. Greif, R.E. Russo, Expansion of the laser ablation vapor plume into a background gas. i. analysis, J. Appl. Phys. 101 (2) (2007), https://doi.org/10.1063/1.2431080.
[194] J. Ho, C. Grigoropoulos, J. Humphrey, Gas dynamics and radiation heat transfer in the vapor plume produced by pulsed laser irradiation of aluminum, J. Appl. Phys. 79 (9) (1996) 7205–7215, https://doi.org/10.1063/1.361436.
[195] A. Gusarov, A. Gnedovets, I. Smurov, Two-dimensional gas-dynamic model of laser ablation in an ambient gas, Appl. Surf. Sci. 154 (2000) 66–72, https://doi.org/10.1016/S0169-4332(99)00389-X.
[196] V.I. Babushok, F.C. DeLucia, P.J. Dagdigian, M.J. Nusca, A.W. Miziolek, Kinetic modeling of the laser-induced breakdown spectroscopy plume from metallic lead, Appl. Opt. 42 (30) (2003) 5947–5962, https://doi.org/10.1364/AO.42.005947.
[197] A. Casavola, G. Colonna, M. Capitelli, Kinetic model of titanium laser induced plasma expansion in nitrogen environment, Plasma Sources Sci. Technol. 18 (2) (2009) 025027, https://doi.org/10.1088/0963-0252/18/2/025027.
[198] S.V. Shabanov, I.B. Gornushkin, Modeling chemical reactions in laser-induced plasmas, Appl. Phys. A 121 (2015) 1087–1107, https://doi.org/10.1007/s00339-015-9445-0.
[199] I.B. Gornushkin, P. Sennikov, R. Kornev, A. Ermakov, V. Shkrunin, Laser induced dielectric breakdown for chemical vapor deposition by hydrogen reduction of volatile boron halides bcl 3 and bf 3, Plasma Chem. Plasma Process. 40 (2020) 1145–1162, https://doi.org/10.1007/s11090-020-10096-w.
[200] S. Shabanov, I. Gornushkin, Chemistry in laser-induced plasmas at local thermodynamic equilibrium, Appl. Phys. A 124 (2018) 1–21, https://doi.org/10.1007/s00339-018-2129-9.
[201] H.M. Urbassek, D. Sibold, Gas-phase segregation effects in pulsed laser desorption from binary targets, Phys. Rev. Lett. 70 (12) (1993) 1886, https://doi.org/10.1103/PhysRevLett.70.1886.
[202] E.A. Lalla, et al., Combined spectroscopic analysis of terrestrial analogs from a simulated astronaut mission using the laser-induced breakdown spectroscopy (LIBS) Raman sensor: implications for mars, Appl. Spectrosc. 75 (9) (sep 2021) 1093–1113, https://doi.org/10.1177/00037028211016892.
[203] T.E. Itina, J. Hermann, P. Delaporte, M. Sentis, Laser-generated plasma plume expansion: combined continuous-microscopic modeling, Phys. Rev. E 66 (6) (2002) 066406, https://doi.org/10.1103/PhysRevE.66.066406.
[204] P.B. Hansen, et al., Modeling of time-resolved libs spectra obtained in martian atmospheric conditions with a stationary plasma approach, Spectrochim. Acta, Part B 178 (2021) 106115, https://doi.org/10.1016/j.sab.2021.106115.
[205] S. Shabanov, I. Gornushkin, J. Winefordner, Radiation from asymmetric laser-induced plasmas collected by a lens or optical fiber, Appl. Opt. 47 (11) (2008) 1745–1756, https://doi.org/10.1364/AO.47.001745.
[206] B.A. Cohen, J.S. Miller, Z.H. Li, T.D. Swindle, R.A. French, The potassium-argon laser experiment (karle): in situ geochronology for planetary robotic missions, Geostand. Geoanal. Res. 38 (2014) 421–439, https://doi.org/10.1111/j.1751-908X.2014.00319.x, 12.
[207] Y. Cho, et al., An in-situ k-ar isochron dating method for planetary landers using a spot-by-spot laser-ablation technique, Planet. Space Sci. 128 (9 2016) 14–29, https://doi.org/10.1016/j.pss.2016.05.004.
[208] F. Cattani, et al., In-situ k-ar dating on mars based on uv-laser ablation coupled with a libs-qms system: development, calibration and application of the karmars instrument, Chem. Geol. 506 (2 2019) 1–16, https://doi.org/10.1016/j.chemgeo.2018.12.010.
[209] J. Gonzalez, Laser ablation-based techniques–data fusion, Chemom. Numer. Methods LIBS (2022) 321–346, https://doi.org/10.1002/9781119759614.ch14.
[210] H. Qin, Z. Lu, S. Yao, Z. Li, J. Lu, Combining laser-induced breakdown spectroscopy and fourier-transform infrared spectroscopy for the analysis of coal properties, J. Anal. At. Spectrom. 34 (2 2019) 347–355, https://doi.org/10.1039/c8ja00381e.
[211] R.C. Wiens, et al., Combined remote mineralogical and elemental identification from rovers: field and laboratory tests using reflectance and laser-induced breakdown spectroscopy, J. Geophys. Res. Planets 107 (11) (2002), https://doi.org/10.1029/2000je001439.
[212] R. Fuentes, et al., Data fusion of laser induced breakdown spectroscopy and diffuse reflectance for improved analysis of mineral species in copper concentrates, Miner. Eng. 173 (2021) 11, https://doi.org/10.1016/j.mineng.2021.107193.
[213] G.R. Peter, de Haseth A. James, Fourier Transform Infrared Spectrometry, vol. 1, John Wiley & Sons, Ltd, June 2007, https://doi.org/10.1002/047010631X.
[214] K. Kawaguchi, et al., Time-resolved fourier transform infrared emission spectroscopy of laser ablation products, Chem. Phys. Lett. 463 (1–3) (SEP 22 2008) 38–41, https://doi.org/10.1016/j.cplett.2008.08.018.
[215] S. Civiš, V. Chernov, Time-resolved fourier transform infrared emission spectroscopy: application to pulsed discharges and laser ablation, in: G. Nikolic (Ed.), Fourier Transforms – Approach to Scientific Principles, InTech, 2011 (chapter 11).
[216] J. Moros, M.M. Elfaham, J. Javier Laserna, Dual-spectroscopy platform for the surveillance of mars mineralogy using a decisions fusion architecture on simultaneous LIBS-Raman data, Anal. Chem. 90 (3) (feb 2018) 2079–2087, https://doi.org/10.1021/acs.analchem.7b04124.
[217] J. Wang, et al., Novel combined instrumentation for laser-induced breakdown spectroscopy and Raman spectroscopy for the in situ atomic and molecular analysis of minerals, Instrum. Sci. Technol. 47 (5) (sep 2019) 564–579, https://doi.org/10.1080/10739149.2019.1608236.
[218] A. Nardecchia, A. de Juan, V. Motto-Ros, C. Fabre, L. Duponchel, LIBS and Raman image fusion: an original approach based on the use of chemometric methodologies, Spectrochim. Acta, Part B 198 (dec 2022), https://doi.org/10.1016/j.sab.2022.106571.
[219] G. Guo, et al., Integrated instrumentation for combined laser-induced breakdown and Raman spectroscopy, Instrum. Sci. Technol. 47 (7 2019) 355–373, https://doi.org/10.1080/10739149.2018.1564052.
[220] S. Schröder, et al., Effects of pulsed laser and plasma interaction on fe, ni, ti, and their oxides for libs Raman analysis in extraterrestrial environments, J. Raman Spectrosc. 51 (9 2020) 1667–1681, https://doi.org/10.1002/jrs.5650.
[221] J.A. Manrique-Martinez, et al., Evaluation of multivariate analyses and data fusion between Raman and laser-induced breakdown spectroscopy in binary mixtures and its potential for solar system exploration, J. Raman Spectrosc. 51 (9 2020) 1702–1717, https://doi.org/10.1002/jrs.5819.
[222] P. Sobron, A. Wang, A planetary environment and analysis chamber (peach) for coordinated Raman-libs-ir measurements under planetary surface environmental conditions, J. Raman Spectrosc. 43 (2012) 212–227, https://doi.org/10.1002/jrs.3017.
[223] S.M. Clegg, et al., Planetary geochemical investigations using Raman and laser-induced breakdown spectroscopy, Appl. Spectrosc. 68 (2015) 925–936, https://doi.org/10.1366/13-07386, 9.
[224] S. Choi, D. Kim, J. Yang, J.J. Yoh, Accuracy enhancement of Raman spectroscopy using complementary laser-induced breakdown spectroscopy (libs) with geologically mixed samples, Appl. Spectrosc. 71 (4 2017) 678–685, https://doi.org/10.1177/0003702817691289.

[225] Y. Bi, Y. Zhang, J. Yan, Z. Wu, Y. Li, Classification and discrimination of minerals using laser induced breakdown spectroscopy and Raman spectroscopy, Plasma Sci. Technol. 17 (2015) 923–927, https://doi.org/10.1088/1009-0630/17/11/06, 11.
[226] E. Gibbons, R. Léveillé, K. Berlo, Data fusion of laser-induced breakdown and Raman spectroscopies: enhancing clay mineral identification, Spectrochim. Acta, Part B 170 (8) (2020), https://doi.org/10.1016/j.sab.2020.105905.
[227] A. Nardecchia, A. de Juan, V. Motto-Ros, M. Gaft, L. Duponchel, Data fusion of libs and pil hyperspectral imaging: understanding the luminescence phenomenon of a complex mineral sample, Anal. Chim. Acta 1192 (2) (2022), https://doi.org/10.1016/j.aca.2021.339368.
[228] M. Veneranda, et al., Application of chemometrics on Raman spectra from mars: recent advances and future perspectives, J. Chemom. (2022), https://doi.org/10.1002/cem.3438.
[229] F. Ma, C. Du, Y. Zhang, X. Xu, J. Zhou, Libs and ftir–atr spectroscopy studies of mineral–organic associations in saline soil, Land Degrad. Dev. 32 (2 2021) 1786–1795, https://doi.org/10.1002/ldr.3829.
[230] I. Noda, Advances in two-dimensional correlation spectroscopy (2dcos), in: Frontiers and Advances in Molecular Spectroscopy, Elsevier, 2017, pp. 47–75, https://doi.org/10.1016/B978-0-12-811220-5.00002-2.
[231] K.A.S. Fessler, A. Waldron, A. Colón, J.C. Carter, S.M. Angel, A demonstration of spatial heterodyne spectrometers for remote libs, Raman spectroscopy, and 1d imaging, Spectrochim. Acta, Part B 179 (5) (2021), https://doi.org/10.1016/j.sab.2021.106108.
[232] H.B. Niemann, et al., Composition of titan's lower atmosphere and simple surface volatiles as measured by the cassini-huygens probe gas chromatograph mass spectrometer experiment, J. Geophys. Res. Planets 115 (E12) (2010), https://doi.org/10.1029/2010JE003659.
[233] N. Fray, et al., High-molecular-weight organic matter in the particles of comet 67p/churyumov–gerasimenko, Nature 538 (7623) (2016) 72–74, https://doi.org/10.1038/nature19320.
[234] T.G. Brockwell, et al., The mass spectrometer for planetary exploration (maspex), in: 2016 IEEE Aerospace Conference, IEEE, 2016, pp. 1–17.
[235] M. Holá, et al., Dual imaging of uranium ore by laser ablation inductively coupled plasma mass spectrometry and laser induced breakdown spectroscopy, Spectrochim. Acta, Part B 186 (2021) 12, https://doi.org/10.1016/j.sab.2021.106312.
[236] M. Dong, et al., Elemental analysis of coal by tandem laser induced breakdown spectroscopy and laser ablation inductively coupled plasma time of flight mass spectrometry, Spectrochim. Acta, Part B 109 (may 2015) 44–50, https://doi.org/10.1016/j.sab.2015.04.008.
[237] A. Makarov, Electrostatic axially harmonic orbital trapping: a high-performance technique of mass analysis, Anal. Chem. 72 (6) (2000) 1156–1162, https://doi.org/10.1021/ac991131p.
[238] C. Briois, et al., Orbitrap mass analyser for in situ characterisation of planetary environments: performance evaluation of a laboratory prototype, Planet. Space Sci. 131 (2016) 33–45, https://doi.org/10.1016/j.pss.2016.06.012.
[239] I. Zymak, et al., A high-resolution mass spectrometer for the experimental study of the gas composition in planetary environments: first laboratory results, Aerospace 10 (6) (2023) 522, https://doi.org/10.3390/aerospace10060522.
[240] A. Sanderink, et al., Olympia-lilbid: a new laboratory setup to calibrate spaceborne hypervelocity ice grain detectors using high-resolution mass spectrometry, Anal. Chem. 95 (7) (2023) 3621–3628, https://doi.org/10.1021/acs.analchem.2c04429.
[241] T. Dequaire, et al., Analysis of carbon and nitrogen signatures with laser-induced breakdown spectroscopy; the quest for organics under mars-like conditions, Spectrochim. Acta, Part B 131 (2017) 8–17, https://doi.org/10.1016/j.sab.2017.02.015, 5.
[242] T. Delgado, L. García-Gómez, L.M. Cabalín, J.J. Laserna, Investigation on the origin of molecular emissions in laser-induced breakdown spectroscopy under mars-like atmospheric conditions of isotope-labeled compounds of interest in astrobiology, Spectrochim. Acta, Part B 179 (5) (2021), https://doi.org/10.1016/j.sab.2021.106114.
[243] D.M. Anderson, et al., Mass spectrometric analysis of organic compounds, water and volatile constituents in the atmosphere and surface of mars: the viking mars lander, Icarus 16 (1) (1972) 111–138, https://doi.org/10.1016/0019-1035(72)90140-6.
[244] T. Delgado, J.M. Vadillo, J.J. Laserna, Laser-induced plasma spectroscopy of organic compounds. understanding fragmentation processes using ion-photon coincidence measurements, J. Anal. At. Spectrom. 28 (2013) 1377–1384, https://doi.org/10.1039/c3ja50147g, 9.
[245] T. Delgado, J.M. Vadillo, J.J. Laserna, Primary and recombined emitting species in laser-induced plasmas of organic explosives in controlled atmospheres, J. Anal. At. Spectrom. 29 (2014) 1675–1685, https://doi.org/10.1039/c4ja00157e.
[246] D. Vaniman, et al., Ceramic ChemCam calibration targets on mars science laboratory, Space Sci. Rev. 170 (1–4) (2012) 229–255, https://doi.org/10.1007/s11214-012-9886-0.
[247] C. Fabre, et al., In situ calibration using univariate analyses based on the onboard ChemCam targets: first prediction of Martian rock and soil compositions, Spectrochim. Acta, Part B 99 (sep 2014) 34–51, https://doi.org/10.1016/j.sab.2014.03.014.
[248] A. Fayyaz, et al., Analysis of rare earth ores using laser-induced breakdown spectroscopy and laser ablation time-of-flight mass spectrometry, Minerals 13 (6) (jun 2023) 787, https://doi.org/10.3390/min13060787.
[249] N. Ahmed, M. Abdullah, R. Ahmed, N.K. Piracha, M.A. Baig, Quantitative analysis of a brass alloy using cf-libs and a laser ablation time-of-flight mass spectrometer, Laser Phys. 28 (1) (2018), https://doi.org/10.1088/1555-6611/aa962b.
[250] A. Fernandez, X. Mao, W. Chan, M. Shannon, R.E. Russo, Correlation of spectral emission intensity in the inductively coupled plasma and laser-induced plasma during laser ablation of solid samples, Anal. Chem. 67 (14) (1995) 2444–2450, https://doi.org/10.1021/ac00110a020.
[251] M. Dong, et al., Coal discrimination analysis using tandem laser-induced breakdown spectroscopy and laser ablation inductively coupled plasma time-of-flight mass spectrometry, Anal. Chem. 92 (2020) 7003–7010, https://doi.org/10.1021/acs.analchem.0c00188, 5.
[252] J.L. Gottfried, R.S. Harmon, F.C. De Lucia Jr., A.W. Miziolek, Multivariate analysis of laser-induced breakdown spectroscopy chemical signatures for geomaterial classification, Spectrochim. Acta, Part B 64 (10) (2009) 1009–1019, https://doi.org/10.1016/j.sab.2009.07.005.
[253] B.E. Boser, I.M. Guyon, V.N. Vapnik, A training algorithm for optimal margin classifiers, in: Proceedings of the Fifth Annual Workshop on Computational Learning Theory, 1992, pp. 144–152.
[254] Z.A. Umar, U. Liaqat, R. Ahmed, M.A. Baig, Classification of nephrite using calibration-free laser induced breakdown spectroscopy (cf–libs) with comparison to laser ablation–time-of-flight–mass spectrometry (la–tof–ms), Anal. Lett. 53 (2020) 203–216, https://doi.org/10.1080/00032719.2019.1643359.
[255] K. Song, et al., Characterization of laser-induced plasma in a vacuum using laser ablation mass spectrometry and laser-induced breakdown spectrometry, Microchem. J. 76 (2004) 95–103, https://doi.org/10.1016/j.microc.2003.10.014, 2.